



Title	Transportation Network Optimisation during Exploratory Migration in Physarum polycephalum
Author(s)	Schenz, Daniel Thorsten
Citation	北海道大学. 博士(生命科学) 甲第13606号
Issue Date	2019-03-25
DOI	10.14943/doctoral.k13606
Doc URL	http://hdl.handle.net/2115/74323
Type	theses (doctoral)
File Information	Daniel_Thorsten_Schenz.pdf



[Instructions for use](#)

Transportation Network Optimisation
during Exploratory Migration
in *Physarum polycephalum*

Daniel Thorsten SCHENZ

Graduate School of Life Science, Hokkaido University

2019, March

Contents

Abstract	v
1 Introduction	1
2 <i>Physarum polycephalum</i> and mathematical models describing its behaviour	5
2.1 Structure and life style	5
2.1.1 Culturing practice	8
2.2 Properties and models	8
2.2.1 The network adapts to flows	9
2.2.2 Contraction waves	12
2.2.3 The growth front	20
3 Network formation during extension	23
3.1 Tube network dynamics during exploration – experimental evidence	23
3.1.1 Materials and methods	24
3.1.2 Statistical analysis	26
3.1.3 Results – a characteristic centre-in-centre trajectory	26
3.1.4 Discussion – achieving global efficiency	30
3.2 Centre-in-centre vein trajectory and the Physarum Solver	37
4 Modeling the network formation during extension	41
4.1 A complex model based on the physiology of the extending slime mould	41
4.1.1 The elements of the model	42
4.1.2 Layers, interactions, time scales, and numerical scheme . .	46
4.1.3 Evaluation of the model	49
4.1.4 Variation of model parameters	54
4.1.5 Interpretation	56
4.2 Derivation of a simple algorithm to predict the vein network’s lay-out	58

4.2.1	Algorithm principle	58
4.2.2	Evaluating the algorithm's performance	61
4.2.3	Conclusion	65
5	Outlook	67
5.1	The biological setting of the current reinforcement dynamics . . .	67
5.2	Generality of the algorithm	68
	Acknowledgements	71
	Bibliography	73

Abstract

Transportation networks of biological systems are essential for enabling efficient mass flow where diffusion alone would be too slow. Thus, they play a central role for an organism’s physiology and a high degree of energetic efficiency has been proposed as a guiding principle for the layouts of these networks. However, it is unclear how they form in a domain that is itself changing (extending) spatially, since at the time of network development, crucial information on the spatial layout of the domain is not yet available. The aim of the present work is to study how a biological transportation network can develop spatial efficiency in a regime of incomplete spatial information.

The true slime mould *Physarum polycephalum* is an apt model organism for studying the development of a transportation network in an expanding domain, because it prominently features an adaptive tube network as it extends over surfaces and we have an understanding of the rules that shape this network, at least in a static situation.

To understand the typical shape and development of the vein network of *Physarum*, we let the organism explore a spatially limited arena, in particular a narrow lane with 90° turns, and observed the position of the main vein relative to the corridor’s edges. In this setting, the slime mould’s main vein, instead of keeping to the centre line of the corridor or being established along the line of the geometrically shortest possible path, cuts the corners and then returns to the centre line. The result is a centre-in-centre line at each corner. This is a striking behaviour that is reproduced well throughout replicates and different arena shapes. However, the lay-out thus realised strikes a good balance between two conflicting measures of efficiency, namely total network length and average network accessibility.

The best-known model of *Physarum* vein development, the ‘Physarum Solver’, works on the premise that the organism has fully extended over the available arena with all possible veins within its domain being of essentially the same diameter. However, this is not the situation we are dealing with during exten-

sion. Running the Physarum Solver model on an arena of the same shape as used in the extension experiments, we therefore find a vein pattern very different from the experimental result. In particular, in that simulation, the single main vein follows the geometrically shortest possible path closely, which pre-supposes global information not available to *Physarum* in a natural setting.

In order to understand the development of the extending tube network in its dynamic environment, we introduce a composite model considering three elements essential to the extension of *Physarum*: the extension of the growth front, the development of the tube network, and the rhythmic contraction waves as a driving force for the cytosolic flux.

The resulting model robustly and accurately re-creates the key features of the organism’s extension: the main veins are formed at a short distance behind the growth front; the position of the main vein, once it has emerged, remains constant over time; and the trajectory of the main vein follows a centre-in-centre pattern at each corner. A variation of the model parameters and the observation of the results suggests that the centre-in-centre geometry is a product of the organism coupling the development of its vein network to the extension of the growth front such that current-reinforcement-based optimisation can work locally, while still allowing for the rapid construction of a tube network.

A corollary of this finding is that growth front extension history alone should be sufficient to make a prediction on the main vein trajectory. To this end we introduce a simple graphical algorithm which is able to predict experimental results with remarkable accuracy. This algorithm is based on very general principles: the local minimisation of connections and the pruning of globally disadvantageous connections due to their carrying less flow. Due to this generality, it would be interesting to see whether the algorithmic formulation can also capture the development of other systems in which the expansion of the system’s boundaries are in step with the construction of its internal network.

In summary, the importance of the growth front expansion for the vein network development had been neglected in previous studies, even though it dynamically determines the area within which the vein network is to be formed. This is relevant since the static situation yields results very different from the dynamic one and is therefore an incomplete and inaccurate description of the biological situation. In addition, the global consequences of a local process such as employed by the current reinforcement model in a dynamic setting are interesting in themselves.

Under the assumptions of the static model, the food sources act as attractors for the body mass of *Physarum* and generate a directional body mass flow

necessary for the current reinforcement mechanism to work. In the more natural setting described here, it is the expansion of the growth front that acts as the body mass sink causing a directional flow. Therefore, we claim that the advantage the current reinforcement mechanism confers to *Physarum* mainly lies in it affording the organism very efficient spatial exploration.

Chapter 1

Introduction

Transportation networks are a ubiquitous feature of biological systems. They play a central role in enabling efficient mass flow over extended domains, where diffusion alone would be too slow [41, 19]. Due to their often considerable size and the necessity to distribute metabolic educts and information as well as collect metabolic products and dispose of them, most multi-cellular organisms feature at least one such network. Vascular plants, as their name suggests, have a phloem system to transport photosynthetic products to their roots and a parallel xylem system that transports water and nutrients to the leaves. These networks can be seen as servicing the two different spheres of plant life and mediating the chemical exchange necessary for their existence. Fungi have (are) a structurally very different network with many redundancies. Their mycelium spans large soil volumes and provides the organism with the ability to distribute nutrients from rich to poor body portions in bundles of parallel hyphae that can handle bi-directional mass flow [18, 23, 31]. Animals show a large diversity of networks both in shape and function. There are of course often different networks for different media such as a pulmonary system for air, a cardiovascular system for blood, a lymphatic system for lymph, and it can be argued that there are even hierarchies of transportation networks such as when social or eu-social organisms construct networks enabling an efficient flow of individuals.

This ubiquity underscores the idea that transportation networks play a central role for an organism's physiology and a high degree of energetic efficiency has been proposed as a guiding principle for the layouts of these networks. Network branching patterns are considered to be physiologically optimised to reduce the energy lost to friction and network maintenance [51], a fact scaling laws for metabolic rates can be based on [87]. Similarly, the routing and the connectivity

of spatial networks have been explained using generalised ‘costs’ and ‘efficiency’ [25]. In addition, the topology of networks can also be understood as the result of a local energy optimisation process [33].

However, these analyses don’t consider the development of the network. Networks of biological organisms are usually not constructed within a fully developed domain, but instead extend together with the growth of the organism’s body. This is most obvious in fungi whose growth means the longitudinal extension of the mycelial network [16, 9]. In plants, the root and branch networks stretch out over the whole life time of the organism, while leaf vein patterns are usually determined in leaf anlagen and stretch and differentiate concurrent with leaf growth [48, 71, 67]. Similarly, the cardiovascular system is laid out in the early stages of embryonic development and grows and undergoes flow-dependent differentiation as the organism gains in size [21, 8]. Neural wiring through axon sprouting, however, is happening in a somewhat more developed organism and even occurs in the adult [26]. It is a highly regulated process in which the axons are guided through the organism to reach their target [78]. But then, the nervous system is not a transportation network and thus the topological lay-out is likely not subject to the same physical requirements.

In summary, transportation networks enable efficient metabolism through their efficient spatial construction. However, they are constructed in a domain that is itself changing (extending) spatially. In other words, at the time of network development, crucial information on the spatial lay-out of the domain is not yet available. *The aim of the present work is to study how a biological transportation network can develop spatial efficiency in a regime of incomplete spatial information.*

To illustrate this point we can imagine an organism with a simple vein structure extending through domains of various shapes, as in figure 1.1, and suppose each of the veins (orange) are efficiently placed (for a given task in a given system). However, the organism has to grow and gradually fill the shape. Assuming the organism is placed at the bottom of each shape and extends towards the top, constructing its vein concurrently with the growth, and assuming the organism has no advance knowledge of the over-all shape of its environment, a seeming dilemma becomes obvious once the organism has reached the stage highlighted in yellow: The organism, has no motivation according to its momentary information to construct the vein anywhere but in the middle, while we know from inspection of the over-all geometry of the arena that the vein should start to swerve towards the direction of the bend in the areas delineated with the broken line, if it is to maintain over-all efficiency. Therefore, one may ask how the

transportation network should be constructed so as to enable an efficient lay-out through all developmental stages as more and more of the arena is discovered.

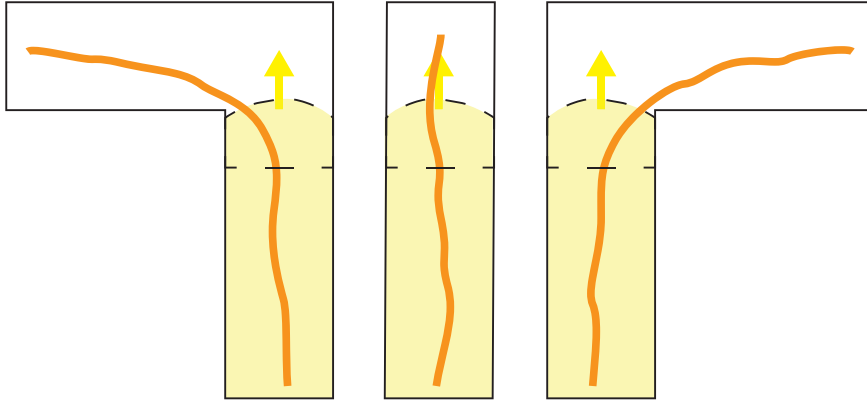


Figure 1.1: Conceptual illustration of the main issue of this work. An organism, which constructs a single vein through its body, extends through a narrow arena, the geometry of which is unknown to the organism until exploration, from the bottom towards the top. Assuming that for each arena shape we know what the ‘optimal’ vein trajectory should look like for the fully extended organism (orange line), at the extension stage highlighted in yellow it is unclear how the vein should be constructed in the area delineated with the broken line, since in all cases the organism has experienced the same geometry this far. There is no motivation to deviate from the centre line, however, not doing so would result in an over-all inefficient vein position.

Uni-cellular, eukaryotic organisms (‘protists’) are an attractive study object for many general questions, especially as regards spatial behaviour [42, 60, 38, 62]. They are subject to many of the same physical constraints as larger organisms and, due to their simplicity, often find quite pure solutions that are showing of trade-offs and interdependences of physical processes. That is to say, their behaviour is easy to model and general rules can readily be found. In addition, they are conveniently cultured in large numbers. However, even though their simplicity makes them attractive, their behaviour is often governed by very basic molecular mechanisms that are also present in our cells.

The true slime mould *Physarum polycephalum* lends itself particularly well to studying the development of a transportation network in an expanding domain, for two reasons. First, it is an easy-to-handle, macroscopic organism that prominently features an adaptive tube network as it extends over surfaces [76,

12]. More importantly, though, we have an understanding of the rules that shape this network, at least in a static situation [81, 35, 15].

For these reasons, we use *Physarum* as a model of a transportation network extending through an extending domain in the present study. Using experimental evidence and results from mathematical models of the organism's behaviour, we demonstrate the ability of local optimisation rules to produce globally efficient solutions.

In the following chapter, we will first introduce *Physarum* as a biological organism and then focus on individual aspects of its physiology that are relevant to its extension and to the formation of its network. We will also review models for each of these aspects. In the third chapter, we will discuss the striking characteristics of the organism's network formed during expansion, but also the shortcomings of present models to explain the behavior. In the fourth chapter we will construct a novel mathematical model and interpret it from a biological point of view. In the last chapter, we will discuss some of the ramifications of the model.

Chapter 2

Physarum polycephalum and mathematical models describing its behaviour

2.1 Structure and life style

Physarum polycephalum is a eukaryotic, uni-cellular organism, a member of the class Myxogastria (‘plasmodial slime moulds’), which are a sister group to the Dictyostelia within the Mycetozoa, part of the Amoebozoa (figure 2.1) [20]. These are a basal eukaryotic group distinct from the plant-containing Diaphoretickes and the Excavata, but a sister group to the Opisthokonta comprising animals and fungi [10, 17].

The life cycle of *Physarum* (figure 2.2) contains a haploid phase that starts with spores being distributed passively. They germinate in moist environments forming uni-nucleated swarm cells. If two such cells fuse and undergo karyogamy, the fusing of nuclei, they produce a diploid plasmodium. In this stage, the organism can undergo synchronous nuclear divisions without cytokinesis, the separation of cell plasma by membranes, and increase in size enormously [49, 74]. After starvation or in UV-radiated environments, the slime mould will sporulate and form sporangia containing haploid spores [39, 49, 11].

The plasmodium deserves a more detailed description, since it is the main object of most *Physarum* studies. The plasmodium expands over surfaces (section 2.2.3) in the search for food, which it engulfs and ingests by endocytosis. In this process, the single cell can span up to 5m² [74], making it the largest cell on record. The body is nerved by a tube network (section 2.2.1), through

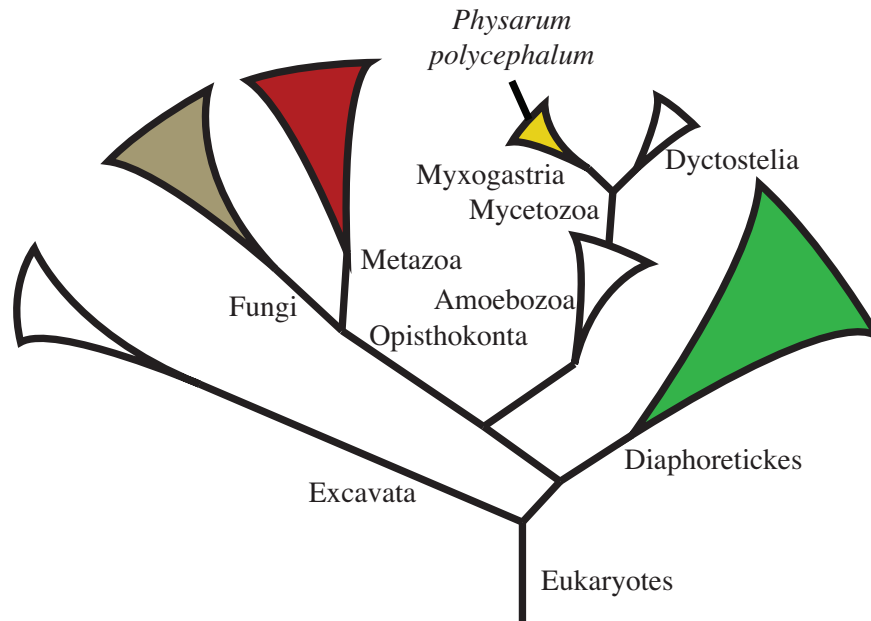


Figure 2.1: Phylogenetic tree of the eukaryotes. The Myxogastria (yellow) containing *Physarum* are a sister group to Dictyostelia within the Mycetozoa, which are a part of the Amoebozoa. These are a sister group to the Opisthokonta which contain the Fungi (ochre) and animals within the Metazoa (red). The Diaphoretickes (green) contain the plants. The Excavata are the most basal Eukaryotes. [10, 17] The branch lengths do not represent anything particular (e.g., time, sequence difference or statistical support).

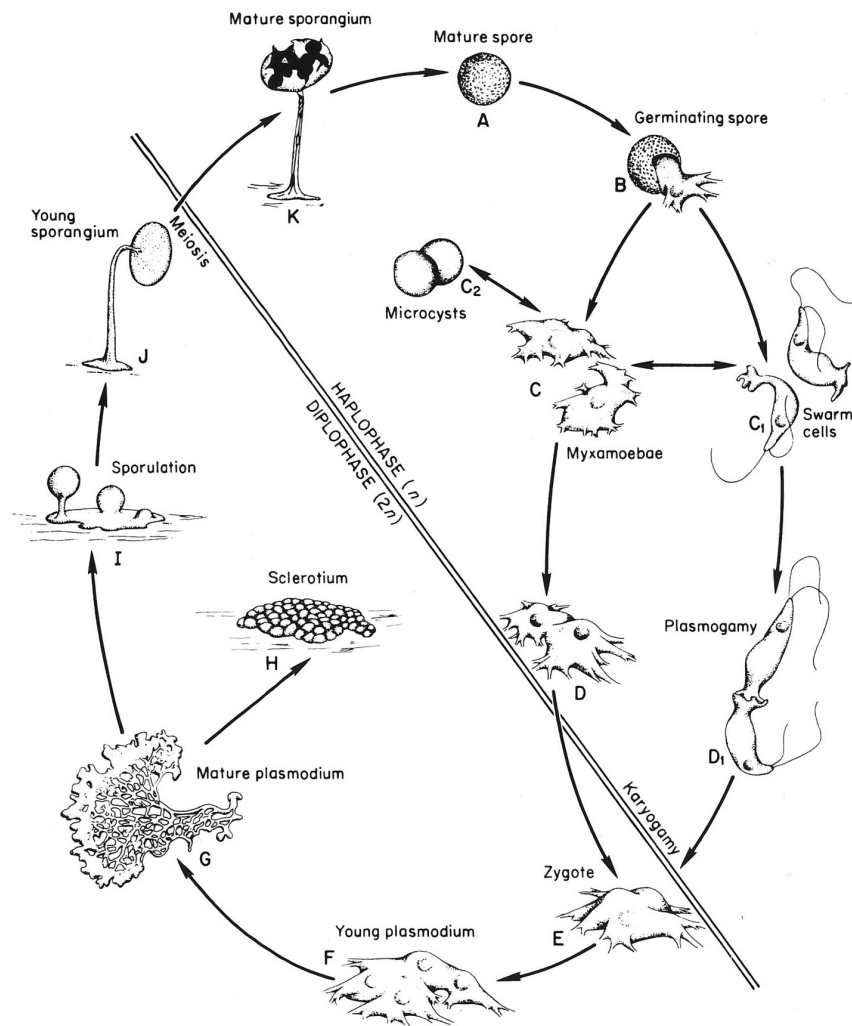


Figure 2.2: Life cycle of *Physarum polycephalum*. From [4].

which cytoplasm is pumped by periodic actomyosin contraction (section 2.2.2). If dried, the plasmodium can form into a hardened state called ‘sclerotium’ in which it can survive for a few years. If re-wetted, a plasmodium will re-emerge from the sclerotium [39].

2.1.1 Culturing practice

In experimental practice, the plasmodium is either grown in liquid culture or on large agar plates. Liquid culture plasmodia are small and spherical (on the order of $100\mu\text{m}$ diameter), and coalesce after being plated onto agar to form small functional plasmodia [13]. Growing *Physarum* plasmodia on large agar plates has the advantage that much more body mass is available for experimental manipulation [85].

For the experiments in this study, we cultured plasmodia on agar plates kept in the dark at room conditions (22°C or 23°C , 30%-60% humidity). To start such a culture, we placed sclerotia, that is, dried plasmodia onto agar plates and re-wetted them with purified water. After a day, a plasmodial sheet re-emerged. We fed the sheet with oat flakes, placing them gently directly onto the growth front. Once the organism has filled the whole plate (measuring $232\times 335\text{mm}^2$), we scattered oat flakes homogeneously and gently over the whole body mass at regular time intervals, with about 8h in-between. This time span is usually enough for the organism to completely engulf the food. When the organism had reached considerable density, after usually 2 or 3 days, we cut the organism together with the underlying agar into (usually 3 or 4) parts and placed them onto new agar. From here we kept the culturing cycle of letting the organism extend over the plate, letting it grow dense, and sub-culturing its parts onto new agar.

For storage, superfluous body mass was placed in a bucket. The plasmodium of *Physarum* climbed the walls clad with wet filter paper over the course of a day, after which we harvested the organism together with the filter paper and placed it in a desiccation box made of cardboard. In these dry conditions, the organism formed a sclerotium.

2.2 Properties and models

In this section we will discuss specific aspects of the plasmodium’s physiology to more detail and introduce models describing each of them. These three models will be the foundation of the synthetic model introduced in section 3.

2.2.1 The network adapts to flows

One of the most prominent features of large plasmodia is the network of veins spanning the organism (figure 2.3 a) [76, 12, 22]. The network transports cytosol from the organism's rear to the front to provide body mass for the extension but also to exchange chemical information between remote body parts [47, 46, 6]. This network also enables the organism to maintain over-all connectivity even if a very small amount of body mass is spread over a physically large area, e.g., to digest multiple food sources (figure 2.3 b) [58].

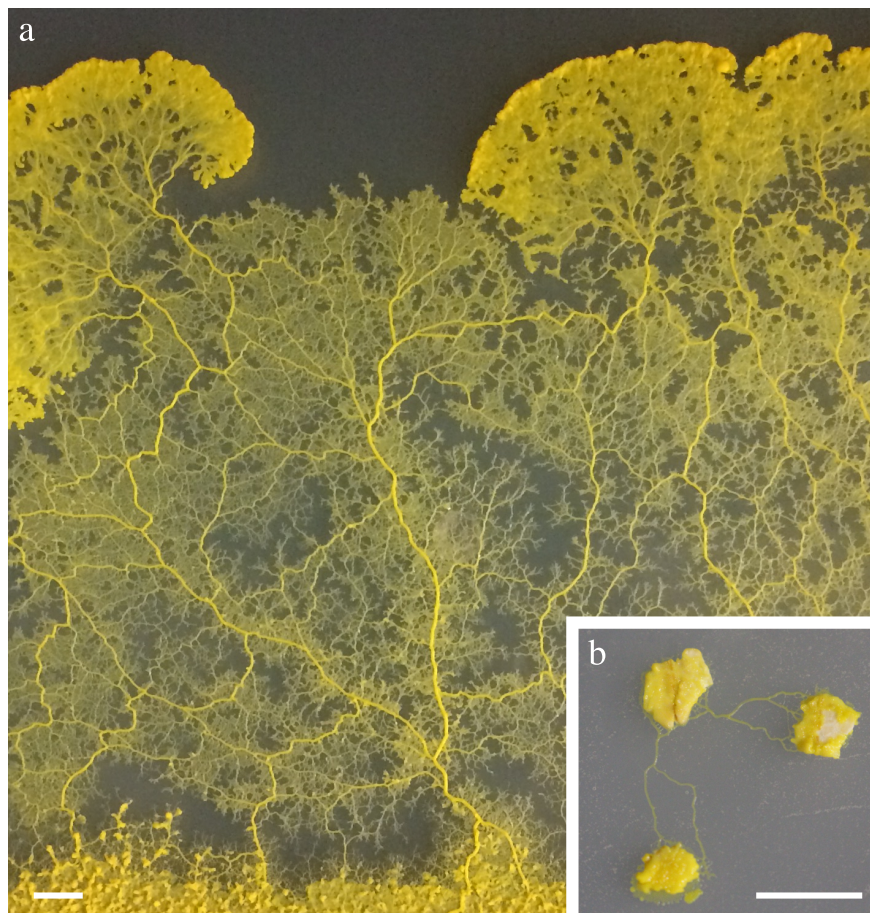


Figure 2.3: Network of *Physarum polycephalum*. a: Tubes span the body mass from the growth front to the rear. b: Even in very small specimens the organism maintains connectivity by its tube network. The bar indicates a length of 10 mm in both figures.

The first anlage of the tube network can be found directly behind the growth front. As the cytoplasm is squeezed through the tube network to extend the growth front, the flow of the more liquid parts (the endoplasm) through the more viscous parts (the ectoplasm) creates proto-channels (figure 2.4 a) [29].

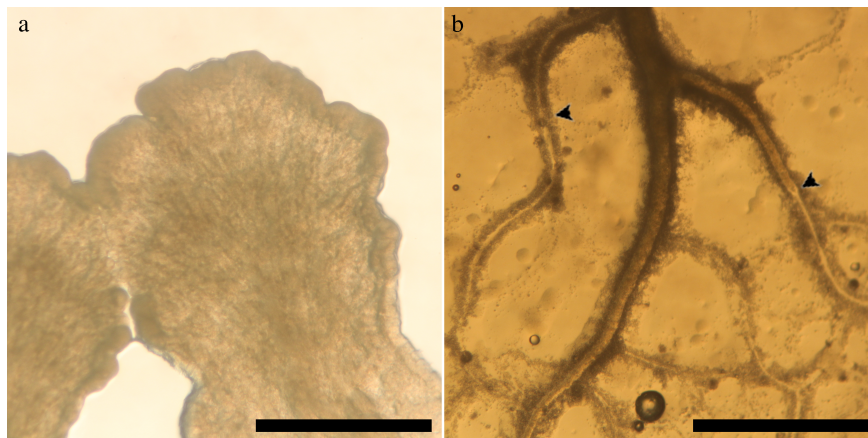


Figure 2.4: Dynamics of the *Physarum* network. a: Tubes are formed by cytosolic flux in the expansion process. This results in many tiny veins that follow the cytosolic flow pattern from the larger veins outward to the growth front. b: In the rear of the organism, tubes are retracted by successive constriction of the tube wall from the rear end (black arrows) forward (in the picture: up) and leave behind a slime pattern in the agar that traces the former position of the veins. The scale bar represents 1mm in both images.

The channels are lined with actin filaments running in parallel to the flow. These actin filaments orient themselves passively in the direction of the flow in a process called shear banding, locally separating the cytoplasm into two fractions with different shear rates. Shear banding also implies that a higher flow velocity should increase the volume fraction of the structure with the lower viscosity, effectively postulating a relationship between the diameter of the vein and the flow through it [44].

On the rear end of the organism the channels are closed and retracted (figure 2.4 b), although this doesn't only occur 'on the other side' of the organism, that is, far away from the growth front, but at all tubes that don't lead to a place of cellular activity [54, 84, 55]. In this way, also tubes relatively close to the growth front that hit a wall or end blind will be contracted until they disappear. This contractility is reminiscent of amoeboid movement and also effected by actomyosin contraction (more on this in section 2.2.2) [39, 52, 5, 80].

This shows that the network is highly dynamic in its ability to respond to the flows it carries. A classic experiment demonstrating this ability is the maze experiment conducted by [54]. The researchers created a maze-shaped arena by placing plastic film onto agar. They then completely filled the arena with *Physarum* plasmodium pieces and placed food sources at two points in the maze. A few hours thereafter, the organism had concentrated its body mass on the food sources but kept them connected with a single tube through the maze. In other words, it had created tubes to evacuate body mass and subsequently retracted all tubes that didn't connect the food sources. Furthermore, the tubes that connected the food sources grew in diameter, with the shorter connections out of all possible connections being chosen statistically more often than others.

These results together hint at a mechanism that exists in *Physarum polycephalum* by which the organism adapts the diameter of its tubes to the flow through it. This is the basis of the current reinforcement rule proposed in [81] and expressed mathematically as

$$\frac{dD}{dT} = f(Q) - kD \quad (2.1)$$

where $D = r^4$ is an expression of the tube diameter, termed 'conductivity' and the fourth power is for convenience (cf. equation (2.3)). Q is the flow through the tube, f is any constantly increasing function, and k is a constant.

This expression of the temporal behaviour of tube diameter as a function of the flow has two terms. The first (positive) term indicates that the diameter increase depends positively on the flow through the tube. The second term is a natural degradation term of the diameter based on the stochastic re-arrangement of the actin filaments that will lead to tube shrinking if it is not counter-acted by flow-induced tube growth. Taken together, the dynamics of the diameter will be dominated by the positive (growth) term in tubes with a relatively high flow, whereas in tubes with relatively low flows the negative (shrinking) term will prevail. The equivalent formulation of the above equation as a relaxation law $dD/dt = -k(D - 1/k f(Q))$ emphasises this interpretation. Here, the system tries to maintain an equilibrium level depending on $f(Q)$. In any case, the result is that current (flow) through a tube reinforces the tube's existence.

Typically, two functions for the flow dependency are considered:

$$f(Q) = a|Q|^\mu \quad (2.2a)$$

$$f(Q) = \frac{|Q|^\mu}{1 + a|Q|^\mu} \quad (2.2b)$$

where μ and a are constants. The parameter μ is significant for the asymptotic behaviour of the system and has experimentally determined as $\mu = 4/3$, which also is in agreement with Murray’s law [3].

The behaviour resulting from equation (2.2a) is more readily analysed analytically. However, the form of equation (2.2b) allows the response of the tube diameter to the flow to saturate. This leads to the possibility of many smaller veins remaining when the flow through the system is large, whereas only a single vein remains when the flow is small. This is in accordance to experimental evidence and is probably the more biologically relevant form [81].

The flow through the tube is assumed to follow the Hagen-Poiseuille relation of flow, tube diameter and tube length (equation (2.3)). This is supported by the flow profile of the cytoplasm, indicating it is transported passively by generation of a pressure gradient across the organism [79, 39, 29].

$$Q = \frac{\pi \Delta P r^4}{8\eta L} \quad (2.3)$$

where Q is again the flow through the tube, ΔP is the pressure difference along the tube, r is the tube’s diameter and L its length. η is the viscosity of the medium. For convenience of equation (2.1), $r^4 := D$, the ‘conductivity’.

These two assumptions automatically suggest a mechanism by which *Physarum* is able to select the shortest possible route through a network out of many alternatives. Comparing two possible routes between the same two points in the organism’s network, which means identical pressure difference, and assuming the tube radii to be equal under initial conditions (and cytosol viscosity not depending on time or tube radius), the flow through the longer tube will be less than through the shorter tube as a consequence of the Hagen-Poiseuille relation. This, following the current reinforcement relation, causes the shorter tube to grow in diameter and the longer tube to shrink, which, in turn, will allow more flow through the shorter tube and less through the longer one.

The above model can be applied to not just a simple network containing two vertices and two edges, but to a complex grid filling an arena with multiple in- and outlets of flow. This is the well-known Physarum Solver model that famously re-created a network very similar to the rail network of the Tokyo Bay area [84, 86].

2.2.2 Contraction waves

The flow through the tube network of *Physarum polycephalum* is driven by contraction waves through the body [39, 52, 5, 80]. At regular intervals of around

once in 2 minutes, the ectoplasm contracts, thus increasing the pressure locally and driving the endoplasm to a portion of plasmodium with lower pressure [56, 65]. The ensuing flow transports cytoplasm through the channels, and because the contractions are periodic and coordinated, the flow changes direction periodically. This is called ‘shuttle streaming’ and facilitates cytoplasmic dispersal and tube formation [46, 6].

The contractions are caused by myosin fibers cross-linking with actin filaments through their head subdomains that can cock and bend repeatedly to exert tension on the actin filament [52, 74]. This process hydrolyses ATP and leads to a contraction of the actomyosin complex.

The regulation of this process in *Physarum* is generally similar to the mechanism in smooth muscle (figure 2.5 a). In both cases, the ATPase is activated by phosphorylation of the myosin light chain regulatory subunit, called ‘LC1’ in the slime mould. This phosphorylation is effected by myosin light chain kinase (MLCK), which is active only if it can bind to a calcium-calmodulin complex. MLCK is itself regulated by another phosphorylation, by protein kinase A (PKA), however, this phosphorylation is inhibitory by drastically reducing MLCK’s affinity to calcium-calmodulin. PKA is activated by cyclic AMP (cAMP), which is, in turn, produced by a calcium-dependent adenylyl cyclase. Together, this means that calcium has on independent time scales an activating and an inhibitory effect on myosin contraction: activating through the activation of MLCK, but inhibitory through the cAMP-mediated activation of PKA. Calcium concentration in the cytoplasm itself, finally, depends on leakage from the vacuole, on active transport to the vacuole (which is up-regulated by a cAMP-dependent kinase), and on the calcium-calmodulin affinity of MLCK (regulated by cAMP-dependent PKA) [91, 73, 36].

In contrast to smooth muscle, however, *Physarum* myosin has its own calmodulin-like calcium-binding site (like in mollusk muscle), called the light chain regulatory subunit ‘LC2’, and calcium binding to this subunit inhibits activation by MLCK. This is to say that calcium, in *Physarum*, directly inhibits contraction [39].

Based on these observations, [73] constructed a mathematical model for a calcium-dependent chemical oscillator regulating the rhythmic contraction in *Physarum* (see figure 2.5 b). This model is the second key element of the synthetic model introduced in section 3. Since it is a spatially 0-dimensional model, all reactions are considered to take place in the same location, leading to a few assumptions that might not reflect biological reality. Specifically, the authors combine MLC and MLCK into one entity, so that calcium binding to MLC-

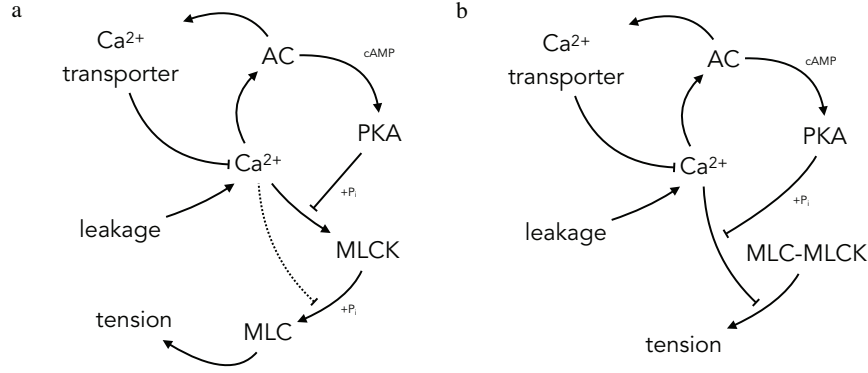


Figure 2.5: Regulation of actomyosin contraction. AC: adenylyl cyclase. PKA: protein kinase A. MLC: myosin light chain. MLCK: myosin light chain kinase. a: Regulation pattern in smooth muscle, including Ca^{2+} -dependent inhibition of MLC phosphorylation by MLCK unique to *Physarum* (dotted line). b: Simplified interaction model used in [73]. This model retains the Ca^{2+} -dependent inhibition of MLC phosphorylation by MLCK as well as the Ca^{2+} -PKA feedback loop. However, the MLC-MLCK complex is treated as if not needing specific activation.

MLCK both regulates contractile tension and is regulated by phosphorylation by PKA.

In mathematical terms, a model can be constructed that describes the changes in the total cytoplasmic calcium levels and the phosphorylation state of the MLCK. These two are the entities driving the oscillator since the phosphorylation state of the MLCK is crucial for the contractile activity of MLC, and the levels of total cytoplasmic calcium are affected only by the exchange with the vacuole but not by fast binding to and release from the MLC-MLCK complex:

$$\begin{aligned} \frac{dc}{dt} &= k_L(N_c - c(t)) - k_V n_c(t) \\ \frac{d\phi}{dt} &= k_Q(n_c(t))(1 - \phi(t)) - k_E \phi(t) \end{aligned} \quad (2.4)$$

where N_c is the total concentration of Ca^{2+} in *Physarum*, c the concentration of cytoplasmic Ca^{2+} , and n_c the concentration of free, unbound cytoplasmic Ca^{2+} . Note that $(N_c - c)$ is the concentration of Ca^{2+} in vacuoles. k_L is the Ca^{2+} leakage rate constant and k_V the rate constant of the Ca^{2+} pump, transporting the ion back into the vacuole. Therefore, the concentration of cytoplasmic Ca^{2+} is determined by leakage of the ion from the vacuole and the active transport

back into the vacuole. The second equation is for the temporal development of ϕ , the fraction of phosphorylated MLCK, where k_Q and k_E are respectively the rate constants for phosphorylation and de-phosphorylation. Note that the rate constant k_Q is a function of the cytoplasmic unbound Ca^{2+} concentration, corresponding to the activation of PKA by Ca^{2+} . The different pools of Ca^{2+} are related through a conservation law:

$$c = n_c + N_M \sum_{k=1}^2 k(q_{ka}(n_c)(1 - \phi) + q_{kb}(n_c)\phi) \quad (2.5)$$

that states that the total cytoplasmic Ca^{2+} concentration c is the sum of the unbound Ca^{2+} n_c and the Ca^{2+} bound to MLC. The latter can bind either zero or one or two atoms of Ca^{2+} per protein and the total concentration of MLC in the cell is N_M . q_{ka} is the fraction of unphosphorylated MLC-MLCK complexes with k Ca^{2+} ions (with $q_{0a} + q_{1a} + q_{2a} = 1$) and q_{kb} is the same for phosphorylated MLC-MLCK complexes. These fractions are determined by:

$$\begin{aligned} q_{ka}(n_c) &= \frac{(K_a n_c)^k}{(1 + K_a n_c)^2} \\ q_{kb}(n_c) &= \frac{(K_b n_c)^k}{(1 + K_b n_c)^2} \end{aligned} \quad (2.6)$$

where K_a and K_b are, respectively, the affinities of unphosphorylated and phosphorylated MLC-MLCK complexes to Ca^{2+} . Since $K_a \gg K_b$, phosphorylation of MLC-MLCK leads to an increase in the proportion of unbound Ca^{2+} n_c . The rate constant for the phosphorylation of MLC-MLCK, finally, is:

$$k_Q(n_c) = k_{Q*} \left(\frac{K_* n_c}{1 + K_* n_c} \right)^\beta \quad (2.7)$$

where k_{Q*} is the maximum rate, K_* is the Michaelis-Menten constant, and β is the Hill constant, so that PKA activity is an increasing function of the levels of Ca^{2+} .

The evaluation of this model is computationally complex and requires sub-algorithms to compute the concentrations of free calcium n_c at each time step. It pays to expand the model into a three-dimensional system with n_c not being

determined by a strict conservation law but by its own dynamical equation:

$$\begin{aligned}\frac{dc}{dt} &= k_L(N_c - c(t)) - k_V n_c(t) \\ \frac{d\phi}{dt} &= k_Q(n_c(t))(1 - \phi(t)) - k_E \phi(t) \\ \frac{dn_c}{dt} &= -k(n_c(t) - (c(t) - A(n_c(t), \phi(t))))\end{aligned}\tag{2.8}$$

where $k \gg O(k_V)$ is a relaxation constant and $A(n_c(t), \phi(t)) = N_M \sum_{k=1}^2 k(q_{ka}(n_c)(1 - \phi) + q_{kb}(n_c)\phi)$ is the concentration of calcium bound to the MLC-MLCK complex. This formulation provides an opportunity to directly model the calcium binding dynamics to that complex while being equivalent to equation (2.5) for all intents and purposes, since the large relaxation constant k will ensure that the difference between the free cytoplasmic calcium n_c and the term $c - A$ will stay practically zero, which will then retrieve the conservation law.

Most importantly, this system can now be analysed with ease (figure 2.6). Using the same parameter values as in [73], the system has one fixed point which is a saddle point with one incoming and two outgoing directions. For all starting conditions of the system variables, the system trajectories quickly converge to a limit cycle in the unstable manifold of the fixed point. A linear stability analysis of the fixed point under variation of the parameters shows that the system has only a small window of values for most parameters where it exhibits non-decaying oscillations. It is quite remarkable that the parameters in [73], many of which were taken from measured values, fall neatly within these windows, because it is by no means obvious that they should enable the expected behaviour. However, the Michaelis-Menten constant K_* for the speed constant of the phosphorylation of the MLCK was chosen arbitrarily and such that it, too, falls within its window of non-decaying oscillations (figure 2.6).

Plotting the nullclines of the system, the reason for this behaviour becomes obvious (see figure 2.7). At the standard value $K_* = 1.5$ (black and grey lines) the system has an unstable fixed point with complex-valued eigenvalues. Owing to $k_Q \gg k_L$ (see section 4.1.2), the vastly different time scales of the equations for $\dot{\phi} = 0$ (fast) and $\dot{c} = 0$ (slow) result in a relaxation oscillation around the fixed point (blue line with green dot as starting values). As K_* is varied, the stability of the fixed point changes as a result of the change in the shape of the nullcline for the proportion of phosphorylated MLC-MLCK complex, ϕ (yellow lines), whereas the nullcline for the cytoplasmic calcium concentration, c (grey line) remains unchanged. This shifts the position of the intersection of the two

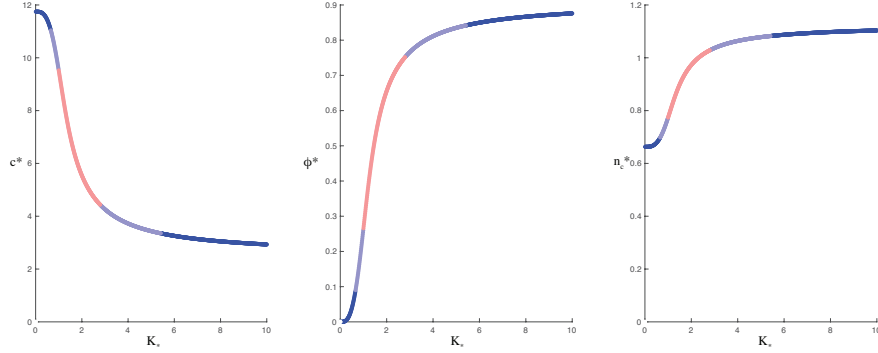


Figure 2.6: Analysis of the fixed point of the three-variable system under variation of a parameter, in this case the Michaelis-Menten constant K_* . Changing this parameter not only shifts the position of the fixed point but also changes its character from stable without oscillations (dark blue) via stable but oscillatory (light blue) to unstable and oscillatory (light red), and back. The parameter value chosen by [73], $K_* = 1.5$, puts the system in the unstable regime, thus allowing bi-stability.

nullclines, that is, the fixed point along the nullcline $\dot{\phi} = 0$, which determines whether or not a relaxation oscillation is possible.

The dynamics of the model (under standard conditions) develop as follows (see figure 2.8). Calcium leaks from vacuoles and starts to inhibit MLCK activity through binding to MLC as well as activation of PKA. MLCK phosphorylation by PKA releases even more calcium, since the phosphorylated MLCK reduces the MLC's affinity to calcium. At this point there is minimal contraction, but the calcium transporters are active and pump calcium into the vacuoles. As calcium levels keep dropping and MLCK becomes increasingly dephosphorylated, MLC affinity for calcium increases as a result, soaking up the remaining calcium. The cell now experiences maximal contraction, however, leaky vacuoles restart the cycle.

The local pressure oscillations produce cytosolic flux to neighbouring regions where the membrane system is passively deformed. This induces mechanosensitive calcium channels to release calcium ions from vacuoles, in the process entraining the local oscillators. Thus, influx-driven stretch entrainment has the ability to couple local oscillators system-wide [39, 7].

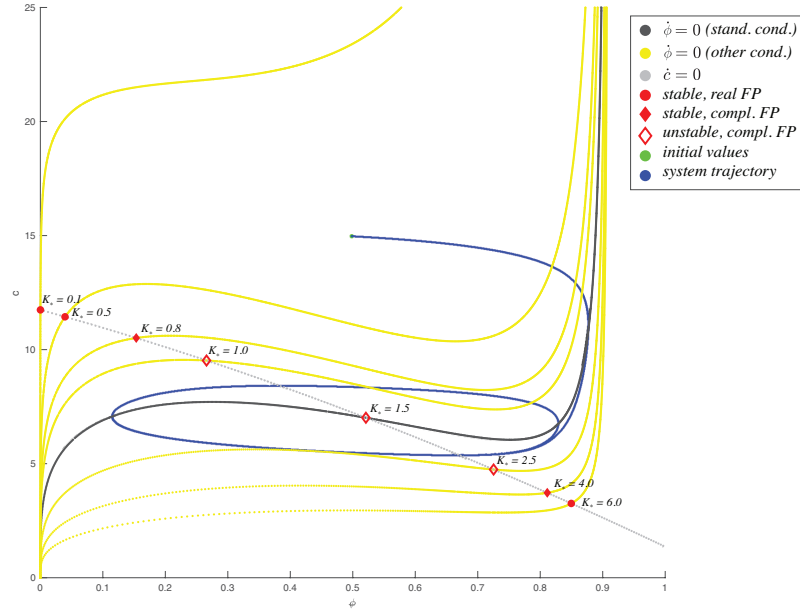


Figure 2.7: The 2-dimensional phase diagram for the proportion of phosphorylated MLC-MLCK complex, ϕ and the cytoplasmic calcium concentration, c . Shown are the nullclines $dc/dt = \dot{c} = 0$ in grey and $d\phi/dt = \dot{\phi} = 0$ in black for the standard condition $K_* = 1.5$ and in yellow for other values of K_* . At the intersections of the nullclines are the system's fixed points (red): circles indicate stable fixed points with real-valued eigenvalues, filled diamonds indicate stable fixed points with complex-valued eigenvalues (leading to dampened oscillations), and open diamonds indicate unstable fixed points with complex-valued eigenvalues (leading to a limit cycle and stable oscillations). For the standard condition, a trajectory is shown in blue with starting values in green.

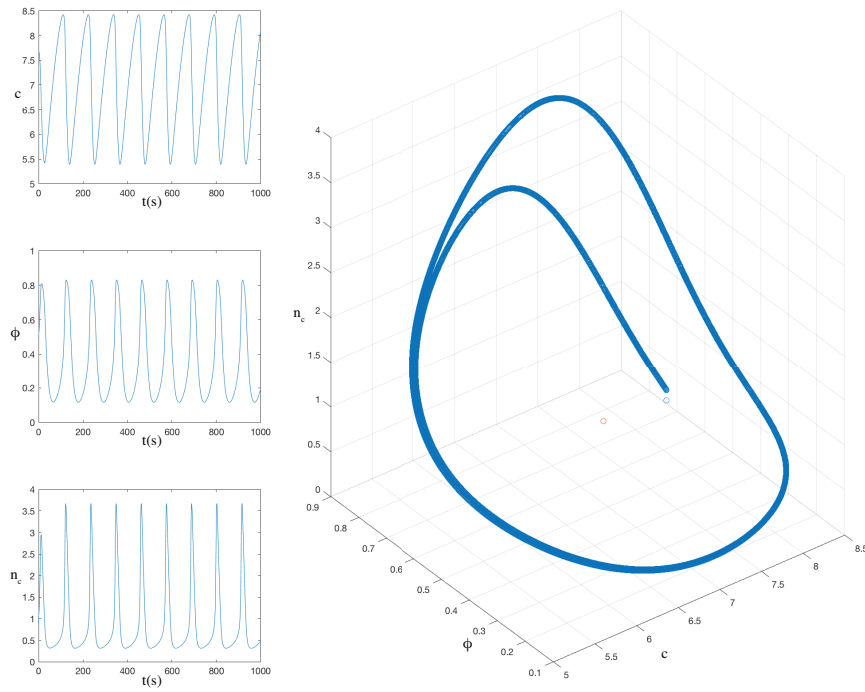


Figure 2.8: Numerical simulation of the three-variable model using the parameter values in [73]. All trajectories (blue) are quickly drawn into a limit cycle around the unstable fixed point (red).

2.2.3 The growth front

While the tube network supplies new biomass to the growth front, the extension of the growth front does not directly depend on the tube network (in the same way as a car's fuel comes from a petrol station, but the petrol station is not directly necessary for the operation of the car). This was clearly demonstrated by amputation experiments in [75]. The researchers let a piece of *Physarum* plasmodium extend through a narrow lane and after a few minutes cut away all of the plasmodial sheet up to a few millimetres at the front, varying the thickness of the piece left between 0.8 and 5 millimetres. Even so, the growth front kept extending for at least another 10 minutes at almost unaffected rates. Notably, the oscillatory contractions (section 2.2.2) ceased immediately upon amputation demonstrating that neither the supply of biomass from the rear nor the contraction waves are immediately required for the extension. However, the growth front became thinner over time and eventually stopped about 20 minutes after amputation [85], which means that supply with cytosol is necessary to sustain extension over prolonged periods.

These findings induced the team to model the propagation of the tip with a one-dimensional reaction-diffusion system based on the transformation of some resource, e.g., sugar into a chemical sustaining the extension, e.g., ATP. The identity of the chemicals involved is not directly relevant, however, since the modelling aim was primarily a spatially propagating chemical transformation that can sustain itself but requires input for long-term survival. Such a polarised chemical pulse can be described well by a Gray-Scott model, which is an auto-catalytic chemical reaction propagating through diffusion of the reaction product to neighbouring regions which 'ignites' the reaction there. A supply term for the educt and an outflow term for the product can be added:

$$\begin{aligned}\frac{\partial u}{\partial t} &= D_u \frac{\partial^2 u}{\partial x^2} - uv^2 + f(1 - u) \\ \frac{\partial v}{\partial t} &= D_v \frac{\partial^2 v}{\partial x^2} + uv^2 - (f + k(x))v\end{aligned}\tag{2.9}$$

where u is the concentration of the resource and v the concentration of the product, the extension-sustaining chemical. D_u and D_v are the diffusive constants of u and v . f , originally termed for 'flow rate' into and out of reaction tanks, is a constant regulating the supply of u into and the efflux of v out of the system. $k(x)$ is a function that allows the system to react to its immediate spatial environment. If $k(x) = k_0$ everywhere, this is an expression of the general environmental conditions affecting the wave propagation, and if $k(x) = k_0 + c$ for

some small interval of x within its domain, this is an expression of locally adverse or, if c is negative, beneficial conditions. Obviously, this system represents an autocatalytic chemical reaction consuming u to produce v . f can be set to 0 if no supply of u is permitted. In this case, the reaction will eventually fully consume u and then stop.

Chapter 3

Network formation during extension

Physarum, in order to forage for potential food sources, has to extend over the available surface [66, 12]. This extension requires the advection of body mass from the rear of the organism to the growth front [5, 29]. Since the transport of body mass takes place in the vein network, the energy efficiency of *Physarum* foraging depends on the lay-out of this tube system [50, 3, 77]. To study how the organism forages efficiently, therefore, we need to understand both how it organises the movement of its body mass itself and the patterns of its locomotive behaviour through space and time.

In the following sections we will discuss, first, an experimental study of how the slime mould constructs its network during locomotion. This will be followed up by the introduction of a mathematical model and a simpler algorithm derived from that model that try to explain the experimental findings. In the last section of this chapter we introduce experimental studies focussing on finding regularities in *Physarum*'s foraging behaviour.

3.1 Tube network dynamics during exploration – experimental evidence

Physarum polycephalum is a remarkable experimental model organism: It is easy to handle, grows quickly, and yet has the potential to exhibit complex and adaptive behaviour [54, 1, 68, 34, 45]. At the same time, its organisational simplicity

as a giant (up to several m^2) coenocyte [39, 74] ensures that behavioural decisions are based on general rules, that is, are made in a distributed fashion.

Thus we use *Physarum*'s unique organisation to uncover general principles that enable emergent but 'smart' behaviours [63, 54, 53, 84]. Our general experimental approach is to submit the organism to conditions in which its potential to exhibiting such behaviours can be exposed. Since any observed behaviours are based on capabilities of the organism even if they are not seen under natural conditions, we assume that they lead us to formulating general rules.

For the study of the emergence of a transportation network in expanding domains, we let *Physarum* extend over a carefully shaped surface. The shape is designed to be complex enough to expose adaptive behaviours, but also simple enough to be able to trace observed behaviours back to specific geometric factors. In more concrete terms, we confine the extension of the organism to a narrow lane that is just wide enough for it to form one or two main veins. That is, we basically restrict the organism to one-dimensional extension [75, 85]. On the other hand, we are interested in the organism's ability to adapt its vein network to a change in growth direction. Therefore, we introduce turns into the lane.

We conducted experiments with a variety of shapes following this pattern (figure 3.1): straight lines (as controls), a wide narrow bend, a narrow round bend, a single orthogonal bend, two consecutive orthogonal bends both into the same direction and into opposite directions, and a complicated combination of orthogonal turns into a snake-shape. None of the lanes contained any food source so as to focus on the explorative behaviour and not confuse it with exploitative behaviour, which can induce dramatic morphological changes [54, 58].

3.1.1 Materials and methods

We cultivated *Physarum polycephalum* in the plasmodium stage at 23°C in the dark on 1%(w/v) agar. The culture was fed with unground oat flakes (Quaker Oats Co.) at regular intervals. Before an experiment a batch of well grown *Physarum* culture was transplanted onto a new agar and let expand over it [85, 69].

For the experiments we used segments of the growth front. These segments were cut with a scalpel, weighed to ensure they were of a defined weight of $20 \pm 2\text{mg}$, and lifted onto a 2%-agar plate bounded by the experimental arena. The arena consisted of a 5mm-wide corridor of various shapes but with a total area of 35mm^2 .

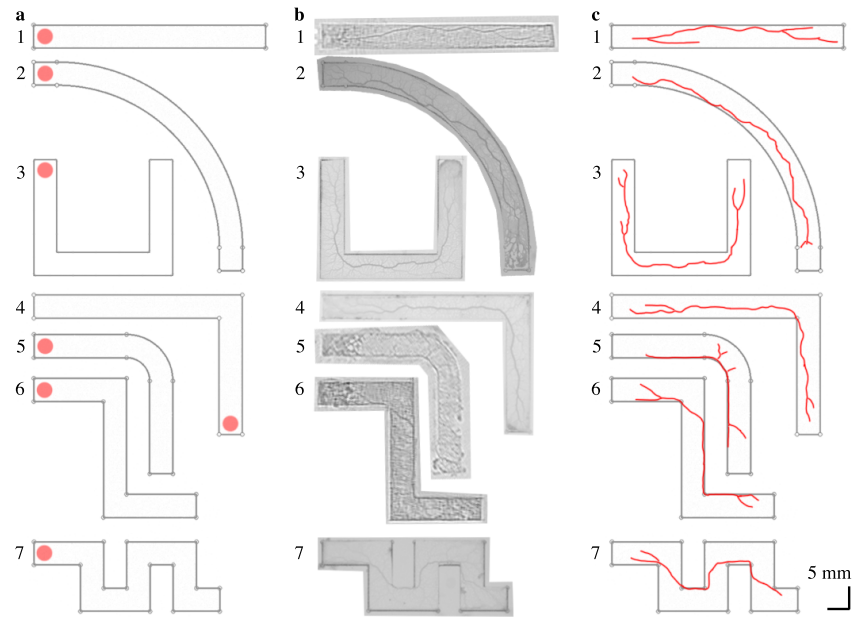


Figure 3.1: Experimental arenas. The lanes are 5 mm wide. a: Shapes. The red dots show where the samples were placed. 1: straight lane; 2: wide round bend; 3: two consecutive orthogonal bends in the same direction ('U-shape'); 4: single orthogonal bend; 5: narrow round bend; 6: two consecutive orthogonal bends in opposite directions; 7: combination of multiple orthogonal bends ('snake shape'). b: Images of representative experimental results. c: Interpretation of the results. The main vein is highlighted in red.

We used 15 replications of a U-shaped arena and 8 replications of a snake-shaped arena. For the duration of the experiment, all dishes were kept in the dark under a slightly opened lid (2mm gap between the lid and the upper edge of the dish). To record the samples' growth, they were placed in-between an infra-red ($\lambda \approx 950\text{nm}$) light source and a CCD camera capturing an image every three minutes (figure 3.2).

In order to ascertain the effect of gravity on the development of the vein network pattern, we mounted 4 of the U-turn arenas horizontally while the other 11 were mounted vertically. Out of these, 5 had the opening of the 'U' pointing downwards and 6 upwards. For the snake shape, all samples were placed horizontally (figure 3.3).

3.1.2 Statistical analysis

To understand the typical exploratory behaviour of *Physarum*, that is, the typical position of its veins when growing in a corridor containing a corner, we evaluated images of the organism's extension through the U-shaped corridor at a stage just after having completely explored the arena. To do this, we measured the distance of the centre of the major vein(s) to the inner boundary at regular intervals of 2mm along the corridor. Then, for each measurement site along the corridor, the respective results across the different samples were averaged to find the average vein position at that site. These averages were then connected with straight lines to estimate the average main vein's course (figure 3.4).

In order to see whether gravity, or rather, the spatial orientation of the organism influences its exploration behaviour, we tested the average vein positions for the different orientations using one-way analysis of variance. At the 95%-significance level, no difference could be found at any point. Therefore, all 15 samples were considered as belonging to the same distribution for further analyses.

3.1.3 Results – a characteristic centre-in-centre trajectory

When growing in the U-shaped corridor containing two 90° turns, the organism's main vein, instead of keeping to the centre line of the corridor or being established along the line of the shortest possible path, cuts the corners and then returns to the centre line. The result is a centre-in-centre line at each corner (figure 3.4).

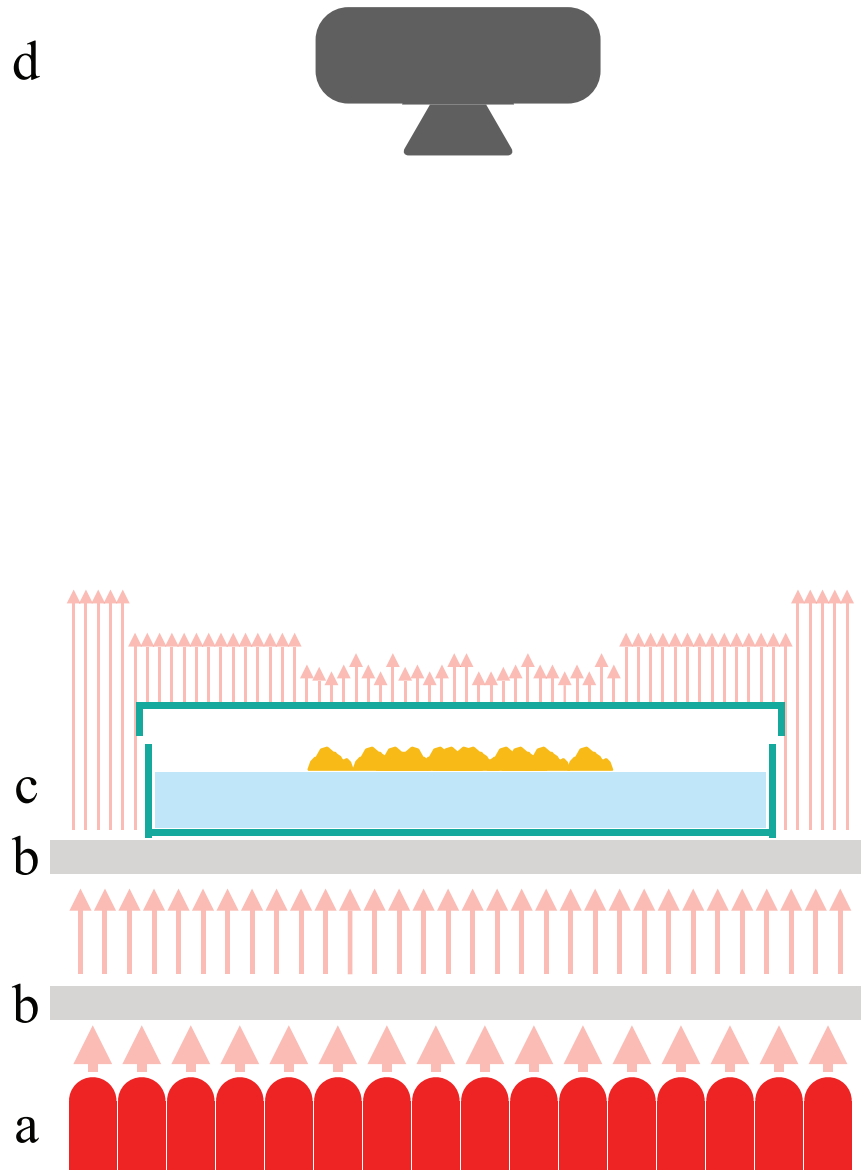


Figure 3.2: Schematic of the experimental set-up. a: Infra-red ($\lambda \approx 950\text{nm}$) LED light source. b: A pair of light diffuser plates to homogenise light. c: The sample is placed on top of the upper diffuser plate. The lid is raised about 2mm above the upper rim of the dish and held in place by tape in three places. This gap prevents condensation on the lid while minimising evaporation. d: CCD camera.

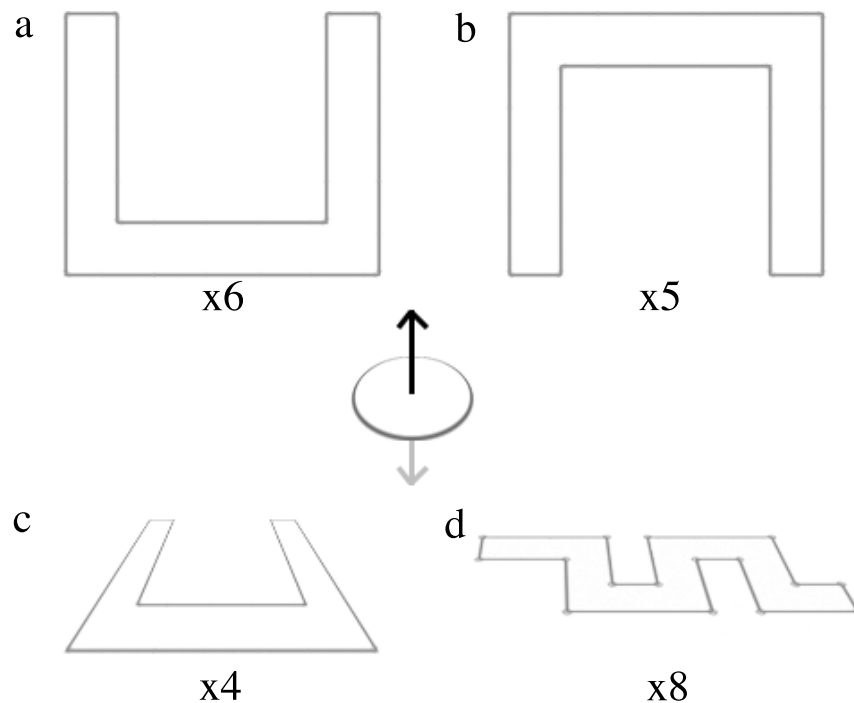


Figure 3.3: Orientation of the plates to test sensitivity of the results to gravitation. a: U-shaped arena with the opening upwards (6 replications). b: U-shaped arena with the opening downwards (5 replications). c: U-shaped arena placed horizontally (4 replications). d: All other samples were placed horizontally only (snake shape: 8 replications).

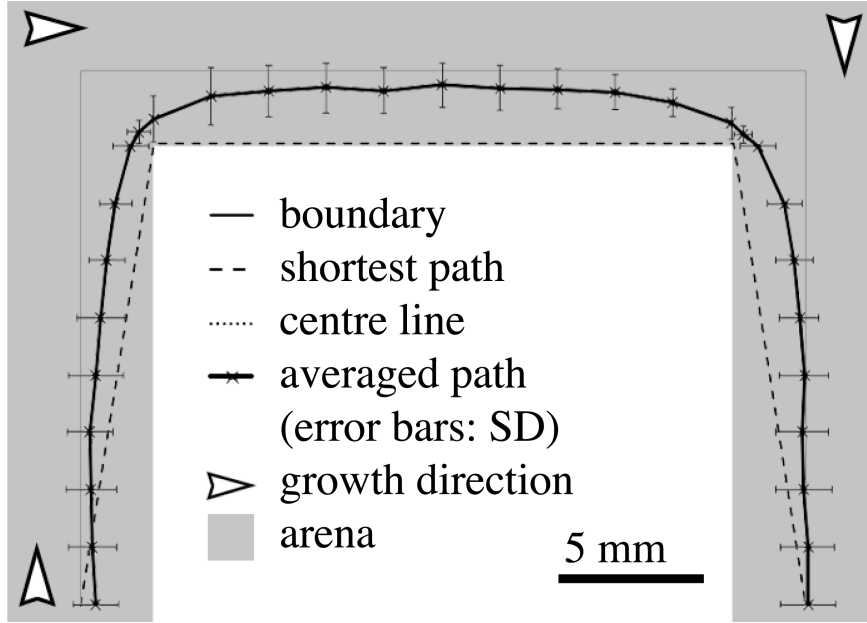


Figure 3.4: Average position of the main vein in experiments with the U-shaped arena. The distance of the main vein from the arena's edge was measured every 2 mm. The resulting average trajectory (solid black line, with standard deviations at each measurement point) is only 6% longer than the geometrically shortest possible path (broken line), while the arena's centre line (dotted line) is 18% longer. The growth direction is indicated by the white arrows. Note the trajectory before, at, and after each corner: The main vein is close to the centre line far a way from the turns, but cuts to the inside of the turn at each corner. We call this trajectory 'centre-in-centre'. See figure 3.5 to see the centre-in-centre trajectory at a single turn. From [69].

This is a striking behaviour that is reproduced well throughout replicates and different arena shapes (also visible in [43, 54, 2]).

Even though the resulting vein is constructed along a clearly distinct line from the shortest possible path, it is only 4.6% longer than the latter over the whole arch (containing two 90° turns).

Analysis of the time series of the exploration showed that it took *Physarum* an average of 15 ± 4 hours to explore the whole arena while the main vein emerges at a spot typically some 50 minutes after the organism has extended its growth front over it. However, in almost all cases the position of the main vein did not change after its emergence (figure 3.5) [43]. In other words, that trajectory had been fixed long before the organism explored the arena fully.

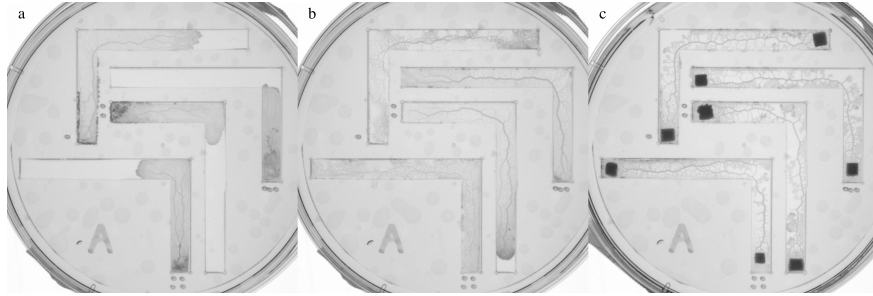


Figure 3.5: Time series example of the experiment. a: 495min after inoculation. b: 1014min after inoculation, just before placing food sources at each end of each lane. c: 2367min after inoculation, 1353min after placing the food sources. The main vein first emerges at a short distance after the growth front (a) and doesn't change its position even after the arena is completely explored (b) or food sources (stimulating flux through the main connecting vein) are available (c).

3.1.4 Discussion – achieving global efficiency

When expanding through a corridor containing a 90° bend, the free-roaming slime mould constructed its vein network with a striking characteristic: The main vein does not follow the centre line of its body, nor does it achieve the globally shortest path. Instead, the organism generally followed the centre line, cut the corners, and then returned to the centre line, thus forming a 'centre-in-centre' trajectory (figure 3.4). This vein network was laid down at a short distance behind the growth front and remained largely unchanged as long as exploration was ongoing, apart from minor side veins gradually disappearing (figure 3.5). In

other words, the vein network lay-out was determined before the global geometry of the arena was ‘known’ to the organism.

How efficient, then, is the result? There are various measures for efficiency of networks, among them average shortest path length, diameter, several definitions of betweenness, and accessibility [14, 28]. Given that the networks produced in our experiments essentially consist of only one vein which may vary in shape and position within the body of *Physarum*, we focus here on length and accessibility.

The total network length determines the efficiency with which body mass can be transported through the main vein. The shortest possible path through the arena used in our experiments would lead the vein along its inner edge between the two bends (broken line in figure 3.4). Compared to this, *Physarum*’s vein is only 4.6% longer. To appreciate this one needs to consider that a path strictly along the centre line (thin line in figure 3.4) would have resulted in a trajectory 18.5% longer than the shortest possible path.

The accessibility, on the other hand, measures the average minimum distance of all points within the arena to the vein. Since a transportation network’s purpose is to service the whole body mass of the organism, it makes sense to construct the vein system such that diffusion distances or transportation through smaller and, therefore, much more resistive vessels are minimised. The best possible vein trajectory in this respect is the centre line. *Physarum polycephalum*’s vein is on average 27.9% farther away from the points within its body. To put this into perspective, the globally shortest path has an average distance 76.4% larger than the centre line.

At this point it should be mentioned that real veins are almost never perfectly straight, but show numerous undulations. This is, however, true for both the actual vein position here and for situations where the organism approaches the globally minimal network length (as in [54, 2, 58]). We therefore deem the underestimation of the path length to be negligible.

Physarum’s vein is not best in either measure, but it strikes a good balance, since probably both dimensions are relevant to the organism’s functioning. If we naively construct a linear combination of both measures of efficiency,

$$E = (w - 1)L + wD \quad (3.1)$$

where E is the combined efficiency (smaller values are better), L is the length of the vein, D the average minimum distance of all points to the vein, and w a weight for the relative importance of the two measures, we can anticipate for which weights *Physarum*’s trajectory would perform better than either of the extreme cases, namely, the globally shortest path and the centre line (figure 3.6).

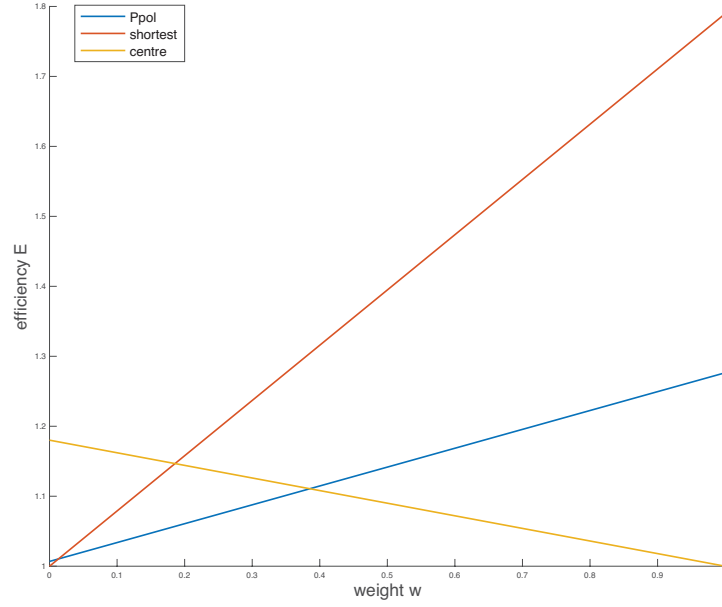


Figure 3.6: A composite measure for efficiency E combining total vein length and average minimum distance between the vein and all points in the body with different weights w . The values for the length were normalised to the length of the globally shortest path, the values for the average minimum distance were normalised to the value for the centre line. The centre line (yellow), the globally shortest path (red) and the vein trajectory of *Physarum* all have a region of weight values of optimal efficiency.

With this approach of simple linear combination of these measures for the efficiency, it is now possible to accurately estimate the relative importance *Physarum* gives to each of these network characteristics. By first asking, for each value of w , which trajectory out of all possible trajectories yields the optimal efficiency, we can search for the trajectories thus obtained for the one closest to *Physarum*'s. The weight corresponding to that trajectory may then be assumed to be an indicator of the weight in the organism as well.

However, it is mathematically difficult and computationally costly to search all possible trajectories. Thus, we performed this search with a piece-wise linear approximation. We chose 9 points, 7 of which are variable, within the arena to serve as anchor points for the trajectory and assumed a straight-line connection between them. We further decreased the number of parameters in the search space by assuming symmetry both between the left and the right side of the arena and between the trajectory directly before and after the 90° turn, thus ending up with only 3 independent parameters (figure 3.7).

We tried 16 values from 0 to 1 for each and all combinations of the parameters a , b and c , resulting in 4,096 different trajectories. For each of these we calculated the length and average minimum distance between the trajectories and all points within the arena. Then we varied the value of the weight w in 151 steps from 0 to 1 and calculated the efficiency for each trajectory. An example for the result can be found in figure 3.8.

Finally, after finding the trajectories with the optimal over-all efficiency for each value of the weight w , we calculated which of these optimal trajectories most closely approximated the trajectory of *Physarum* (see figure 3.9).

The best-fit trajectory was found for a weight $w = 0.167$, which may be interpreted that *Physarum* prioritises the reduction of the total length of the main vein over the optimisation of accessibility, at least in the case of exploratory migration. However, the analysis presented here is very superficial. It can be improved by comparing it to vein trajectories in arenas of different geometry, by including additional measures of efficiency other than just length and average distance, and by generally considering a more physically motivated approach to 'efficiency', that is, calculating a concrete physical dimension such as energetic cost to measure efficiency.

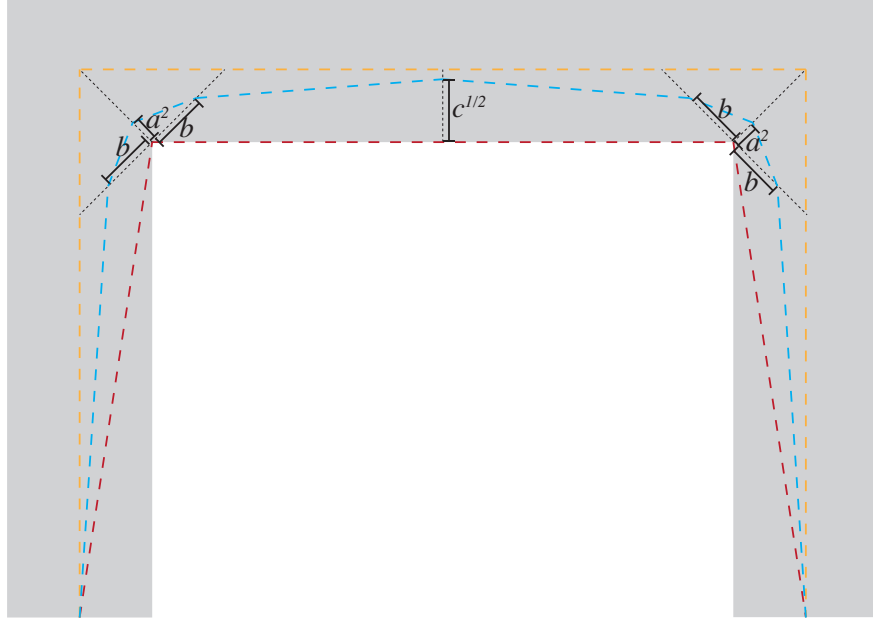


Figure 3.7: The set-up of the piece-wise linear approximation of the total trajectory space to search for the trajectory with optimal combined efficiency for each weight. Within the arena (grey), seven lines (black broken lines) were set up. These lines reach from the inside boundary of the arena to the centre line (but don't extend to the outer boundary). Along each of the lines a parameter (a , b or c) determined the position of the anchor point that would mount the trajectory (red, blue and yellow lines for three different value triplets). Parameters a and c were raised to a power in order to narrow the search spread in certain areas where, from experience, trajectories of *Physarum* could be found more frequently. Note that this is a bias only in accuracy, not in the resulting geometry. Two additional anchor points were fixed at the middle points of the ends of the arena. The red line is the globally shortest path with $a = b = c = 0$, and the yellow line is the centre line with $a = b = c = 1$. The blue line is an example for a trajectory for intermediate values (e.g., $a = 0.4$, $b = 0.6$ and $c = 0.9$).

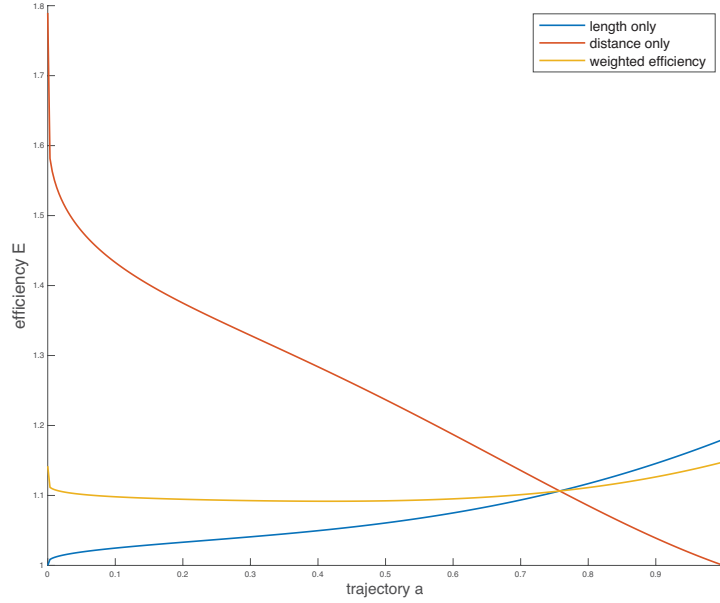


Figure 3.8: One-dimensional example for the results of the calculation of efficiency E for all possible trajectories with only one free parameter a and fixing $b = c = a$ (see figure 3.7 for the definitions). Shown are the results of the over-all efficiency E for $w = 0$ ('length only', blue), $w = 1$ ('distance only', red) and $w = 0.225$ ('weighted efficiency', yellow). It can be seen clearly that in the case where only length is regarded ($w = 0$), the optimal trajectory is found at $a = 0$, which corresponds to the globally shortest trajectory. Likewise, when only distance is considered ($w = 1$), the optimal trajectory has a parameter $a = 1$, which is the centre line. At an intermediate value $w = 0.225$, the optimal trajectory has an intermediate geometry parameter $a = 0.4$.

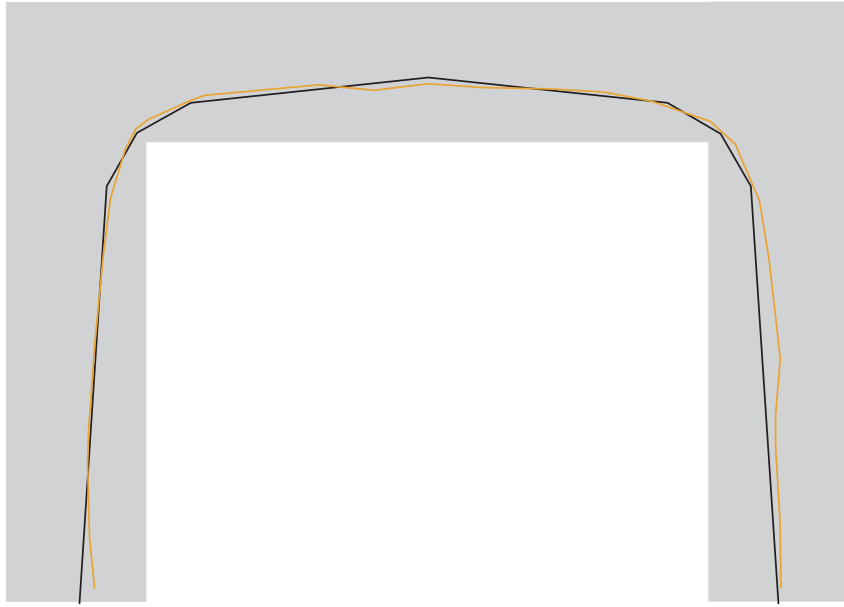


Figure 3.9: Overlay of *Physarum*'s vein trajectory (yellow) and the trajectory with the geometry parameters $a = 0.4$, $b = 0.6$ and $c = 0.933$ (black), which has the optimal over-all efficiency for a weight $w = 0.167$.

3.2 Centre-in-centre vein trajectory and the Physarum Solver

The Physarum Solver developed by [81] is a powerful tool to simulate the development of the vein network of *Physarum* (section 2.2.1). The premise of the model is that the organism has fully extended over the available arena with all possible veins within its domain being of essentially the same diameter. However, this is not the situation we are dealing with in the extension experiments discussed above, where the organism's, and therefore, the network's domain is continuously extending concurrently with the formation of the vein network.

Running the Physarum Solver model on an U-shaped arena, with the end points serving as sources and sinks of the flow, we therefore find a vein pattern very different from the experimental result (figure 3.10). In this simulation, the single main vein follows the geometrically shortest possible path closely. This is best seen in the stretch between the two 90° turns where the vein does not separate from the inner boundary of the arena and, as a consequence, does not produce the typical centre-in-centre pattern at the corners.

This means that the Physarum Solver is able to find the globally optimal solution where *Physarum* does reproducibly not find the shortest possible solution. Nevertheless, the organism is able to come close to it even in the absence of complete information, and the centre-in-centre vein pattern is of key importance to this. The geometric reason for this is that the main contribution to the additional length of a divergence from the globally shortest path comes from the behaviour at the corners. Rounding the corners of a path reduces its length significantly. However, a rounding of corners itself is a local phenomenon, whereas omitting rounded trajectories in favour of sticking to the globally optimal path is obviously only possible under complete spatial information. Therefore, since *Physarum* vein patterns do produce (rounded) centre-in-centre trajectories whereas the Physarum Solver model does not, but finds the global optimum, we have to conclude that the vein network dynamics described by the Physarum Solver model alone are insufficient to capture the mechanism driving the emergence of the vein network during extension.

However, a recent study [2] found centre-in-centre trajectories reproduced by the Physarum Solver model, although the arena used in that publication was much more complex than the ones used here. As a consequence, the appearance of centre-in-centre trajectories depended on the configuration and interaction of neighbouring corners, on the local 'randomness' of the mesh, and on fluctuations in the initial vein thickness (figure 3.11). In other words, the trajectories

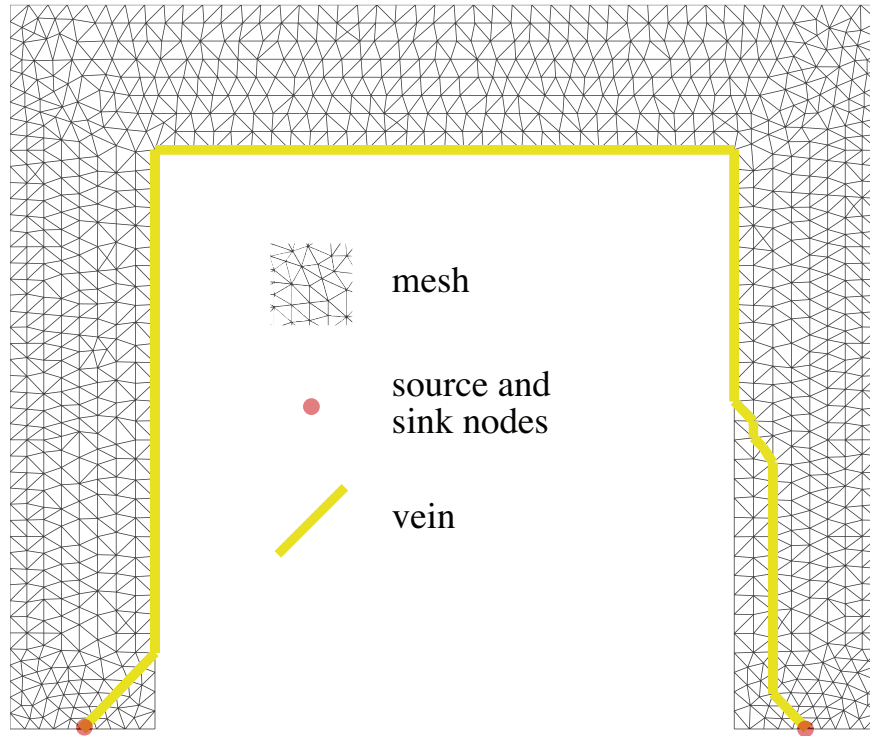


Figure 3.10: The result of a Physarum Solver simulation based solely on the current reinforcement principle. A network spans the whole of the arena. Two points are defined as entry and exit points of some arbitrary flux, the rest of the grid is allowed to adapt its edge diameters to the fluxes. The resulting single vein is the shortest possible path [81]. Most critically, the vein does not return to the centre between the turns. Modified from [69].

found in that study can be considered a result of strict global optimisation under complicated conditions.

Here, however, ‘centre-in-centre trajectory’ means the return of the vein to the centre, unguided by the boundary, after each corner (given sufficient space to do so), even if two consecutive corners turn in the same direction [69]. This is in contradiction to strict global optimisation and can be considered an effect of local optimisation.

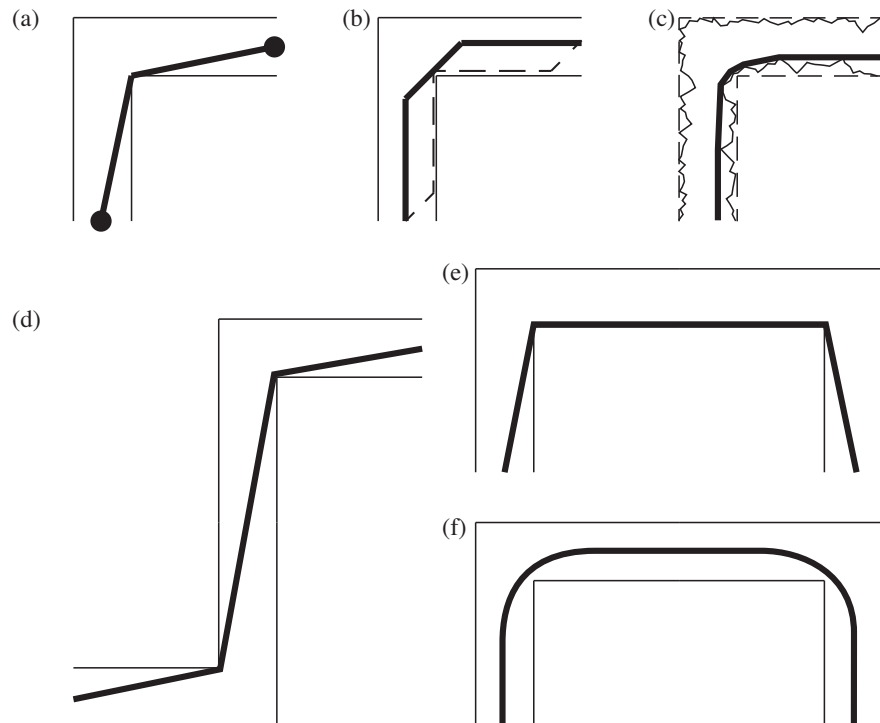


Figure 3.11 (*previous page*): Possible definitions of and causes for a ‘centre-in-centre trajectory’. a: Result of strict global optimisation if starting and ending points are at a distance from the inner boundary. b: In a pre-defined mesh not all trajectories are available. Therefore, there might be a number of trajectories of equal length that are all at the global minimum. Random fluctuations of initial conditions might choose one such trajectory that appears to exhibit the characteristics of a centre-in-centre trajectory (solid line), although other initial conditions might have resulted in a trajectory that is clearly not centre-in-centre (broken line). c: In a random mesh not all space around a corner may be available. In such circumstances, strict global optimisation may produce a trajectory that looks as if it starts from and returns to the centre of the lane, although the reason for this is that a path closer to the inside boundary is simply not available in the mesh. d: Strict global optimisation between orthogonal turns in opposite directions lead to trajectories that cut to the turns’ inside but approach them from the centre line. However, this is a result of the arena’s lay-out. e: If two consecutive turns in the same direction and the space between them are not considered individually, but rather one combined turn, strict global optimisation may lead to a trajectory that follows the inside of the ‘turn’ while starting from and returning to the centre of the lane due to the arena geometry outside of the spot considered. However, the trajectory around each individual corner is clearly not centre-in-centre. f: Only if the trajectory of the vein robustly returns to the centre of the lane even between two consecutive turns in the same direction and even if other choices are available we speak of a ‘centre-in-centre trajectory’. This is the only definition that is in contradiction to global optimisation of path length, allowing us to differentiate between trajectories being optimised globally and locally.

Chapter 4

Modeling the network formation during extension

In this chapter we will introduce two models to recreate the vein trajectory formation of *Physarum polycephalum* during exploratory migration in the absence of food sources. The first model is generative, that is, it is based on certain experimentally determined physiological characteristics, but is not fed with any of the experimental results it is meant to recreate. That is to say, no information on the actual explorative behaviour of the real organism is used in this first model. This will allow us to check which physiological processes and their interactions need to be modeled in order to recreate the behaviour accurately. The second model is based on the understanding gained from the first, but is unrelated in mathematical terms. The quintessence of the relevant building blocks of the first model and their interaction are used to make simple, phenomenological predictions on the trajectory of the vein. However, these predictions are based on the input of some experimental data, specifically, the growth front history. The simplicity of the second model will give us a clear, intuitive understanding of how *Physarum* is able to construct efficient transportation networks during exploratory migration.

4.1 A complex model based on the physiology of the extending slime mould

In order to predict the development of the extending tube network in its dynamic environment, we need a model that can capture the effect of the extension of the

growth front on the development of the tube network. In addition, we model the rhythmic contraction waves of *Physarum* as a driving force for the cytosolic flux through the tube network.

4.1.1 The elements of the model

We employ a composite model [69] consisting of three elements: the growth front, the tube network, and the actomyosin contraction waves, which we will discuss in the given order hereafter. However, while the growth front and the contraction waves can be modelled in continuous two-dimensional space, the tube network has to be modelled on a pre-defined grid of nodes and vertices stretching through the same space.

The growth front

The first element needs to be able to reproduce the behaviour of the growth front. Certainly there is a degree of influence of the rear part of the body on the extension of the frontal tip, if not only for the fact that the body mass necessary for this process is supplied from the rear through the tube network stretching throughout the organism's domain. However, [75] showed that growth front extension can be accurately modelled independently of processes occurring in the rear of the body by a Gray-Scott reaction-diffusion model.

Given that enough body mass is present for the organism to extend throughout the whole of the available arena space, and given that most of the organism's body mass is concentrated in the growth front, it is plausible to model the behavior of the growth front independently from the rear. Thus, we employed the above-mentioned Gray-Scott model (section 2.2.3).

As mentioned there, the physiological interpretation of the reaction-diffusion process, that is, the identification of the model variables with actual chemical species, is at this point only tentative. In the original study [75] introducing a Gray-Scott-type model for the simulation of the growth front behaviour, the model variables were identified as 'intracellular ATP' and 'nutrients'. In a later study [85] they were replaced by 'solation factors' and 'solation regulation factors', the same as used here. In addition we note that in the present implementation of the simulation the concentration of the the solation regulation factors is high even outside the body mass. In other words, these chemicals are modelled as if the pre-existed in the arena. This certainly is not a realistic situation.

How trustworthy, then, is a model which not only includes some clearly unrealistic assumptions, but is not even clear about which conditions are to be

modelled, in the first place? The answer to this question has to be framed from a different point of view: For our purposes, we are looking for a model that can accurately describe the behaviour of the expanding growth front of *Physarum polycephalum*. The only model capable of realistically doing so, to our knowledge, is the above reaction-diffusion-type model. However, it is true that its variables and parameters are not well defined and the model remains a phenomenological one at this level.

The mathematical realisation of the model, equivalent to equations (2.9), is given as

$$\tau_2 \frac{\partial u}{\partial t} = D_u \Delta u - uv^2 \quad (4.1a)$$

$$\tau_2 \frac{\partial v}{\partial t} = D_v \Delta v + uv^2 - \alpha_1 v \quad (4.1b)$$

$$\tau_2 \frac{dw}{dt} = h(v) \quad (4.1c)$$

where u is the concentration of the regulatory factors and v is the concentration of the solation factors. D_u and D_v are their respective diffusion constants and Δ represents the Laplace operator $\partial^2/\partial x^2 + \partial^2/\partial y^2$. α_1 is a positive constant. Supplementing the system given in equations (2.9), the variable w is the organism's thickness, assumed to grow as a function of the presence solation factors $h(v) = \alpha_2 v$, α_2 being another positive constant. τ_2 defines the time scale of the growth front extension relative to the following processes.

The tube network

The aim of the presently proposed model is to accurately describe the development of the tube network in an extending organism. Therefore, a description of the dynamics of the tube system is necessary. The second element of the model is, therefore, a version of the current reinforcement model introduced in [81]. However, we have to adapt the model to work in the context of the extending domain.

Since the growth front is propagating largely independently from the development of the tube network, cytoplasmic flow sinks may not always be available at the same rate as fluid is supplied from the rear – there could either be more flow than the growth front extension can absorb at a given time, or the growth front has expanded more than what can readily be filled by cytosol. In either case, an area of the organism's domain newly made available to the tube network is, in this model, spanned by empty tubes of zero diameter that do not, initially

conduct any flow. Therefore, the tube network must be able to compensate for flow in a pressure-dependent manner by distensible tube walls [64].

As a consequence, the interaction between pressure and flow is not fully captured by the analogy of the electric circuit normally employed for a pure current reinforcement model, with pressure taking the place of voltage and flow the place of current. Instead, the interrelation between pressure and flow is modelled explicitly and individually, and has to incorporate the material properties of the tube.

Together, these dynamics are written in mathematical form as

$$\frac{dq_{ij}}{dt} = \frac{1}{\tilde{I}_{ij}(D_{ij})} \{(p_i - p_j) - \tilde{R}_{ij}(D_{ij})q_{ij}\} \quad (4.2a)$$

$$\frac{dp_j}{dt} = \sum_i \frac{1}{\tilde{C}_{ij}(D_{ij})} q_{ij} \quad (4.2b)$$

$$\frac{dD_{ij}}{dt} = \frac{|q|^\mu}{1 + a_d|q|^\mu} - rD_{ij} \quad (4.2c)$$

where q_{ij} is the flow through a vertex between nodes i and j , and p_i is the pressure at node i . \tilde{I}_{ij} , \tilde{R}_{ij} and \tilde{C}_{ij} are the fluid inductance, resistance and capacitance, respectively, of the tube between nodes i and j . These are model properties of distensible tubes, modified such that they don't diverge at a tube radius of zero, which is the default state of the grid vertices in this model. Inductance, resistance and capacitance are defined respectively as $\tilde{I}_{ij}(D_{ij}) = L_{ij}/(\bar{a}_i + a_i D_{ij}^{1/2})$, $\tilde{R}_{ij}(D_{ij}) = L_{ij}/(\bar{a}_r + a_r D_{ij})$, $\tilde{C}_{ij}(D_{ij}) = (\bar{a}_c + a_c D_{ij}^{3/4})L_{ij}$, where we define $D_{ij}(t) := d_{ij}^4(t)$, d_{ij} being the radius of the tube between nodes i and j , for convenience and will refer to it as 'conductivity'. L_{ij} is the length of the tube. $a_i = 4\pi/9\rho$, $a_r = 8\pi/81\nu$ and $a_c = 2\pi(1-\sigma^2)/(E\theta)$ are constants that are defined by the fluid density ρ , the ordinary coefficient of viscosity ν , Young's modulus for the tube wall E , the thickness of the boundary wall θ and the Poisson ratio for the wall σ . \bar{a}_i , \bar{a}_r and \bar{a}_c are arbitrary constants to generate the saturation terms. The third equation (4.2c) represents the current reinforcement dynamics as in equation (2.1), with a_d and μ being constants controlling the non-linearity of the feedback.

The actomyosin contraction waves

The model for the tube network described in the preceding section is usually realised by choosing, at each iteration, two random nodes in the network's mesh

and designating one as an inlet node and the other as an outlet node with an arbitrary (though fixed) ‘full’ pressure level at the inlet and a zero-pressure level at the outlet. All other nodes have to follow mass conservation for the flows in and out and are assigned pressure values in analogy to assigning voltages to points in an electric circuit.

However, in a situation where the organism is extending more or less unidirectionally over a surface, this implementation is neither practical nor realistic. It is not practical, since the domain changes size at each iteration and, therefore, the chance of choosing a node at the growth front would decrease rapidly over time; it is not realistic, since the over-all flow would not follow a consistent pattern, whereas such a pattern is evidently present in unidirectional extension.

Therefore, flow has to be generated in a different manner than by choosing random inlets and outlets. We achieve this by creating pressure waves that are generated at the starting point for the simulation and propagate throughout the organism. We employ a Smith-Saldana-type model [73] for calcium-driven contraction waves, where the calcium concentration and the phosphorylation state (and, therefore, the activity) of the myosin light-chain kinase influence each other, thus generating a series of self-propagating waves.

The mathematical formulation of the oscillator (cf. equations (2.9)) is

$$\begin{aligned}\tau_1 \frac{\partial c}{\partial t} &= -k_V n_c(c, \varphi) + k_L(N_c - c) + D_c \Delta c \\ \tau_1 \frac{\partial \varphi}{\partial t} &= K_Q(n_c(c, \varphi))(1 - \varphi) - k_E \varphi\end{aligned}\tag{4.3}$$

where c is the concentration of total cytosolic calcium and φ the probability of the myosin light chain kinase (MLCK) being phosphorylated. τ_1 defines the time scale of the contraction waves relative to the dynamics of the growth front and the tube network. k_V and k_L are the respective rate constant for calcium pumping into the vacuole and leakage out of it into the cytosol. N_c is the total calcium concentration in the cell and n_c the concentration of unbound cytosolic calcium, so that $N_c - c$ is the concentration of calcium in the vacuole. D_c is the diffusion constant of calcium and Δ the Laplacian operator as above. k_E is the rate constant of the MLC-MLCK complex de-phosphorylation, whereas the rate of the phosphorylation process K_Q is a function of the free cytosolic calcium concentration n_c (see section 2.2.2), given by $K_Q(n_c) = k_Q[K_* n_c(c, \varphi)/(1 + K_* n_c(c, \varphi))]$. Here, k_Q is the maximum rate of MLC-MLCK phosphorylation and K_* is the Michaelis-Menten constant. The relative quantities, finally, of the total cytosolic calcium c and the free cytosolic calcium n_c depend on the phosphorylation state of the MLC-MLCK

complex and are given by $n_c(c, \varphi) = [1 + 0.17(c - 7.5)](a_0 + a_1\varphi + a_2\varphi^2 + a_3\varphi^3)$ which is a fitted version of equation (2.5) with fitting parameters a_0 , a_1 , a_2 and a_3 [72].

4.1.2 Layers, interactions, time scales, and numerical scheme

The models above fall into two broad categories: the network dynamics are expressed by a discrete model for the dynamics at pre-defined nodes and edges of a planar network. On the other hand, the reaction-diffusion process and the actomyosin contraction waves are descriptions of processes in continuous space. We therefore implement the model as the extension of a continuous ‘organism’ over a discrete and pre-defined network, with the reactions taking place in the appropriate ‘layer’. However, the dynamics of vein formation, actomyosin contraction and leading edge formation interact with each other. There are four such interactions.

(1) The tube network advects chemicals that take part in the reaction-diffusion process in the growth front. As stated earlier, this process, as modelled here, can sustain itself independently due to the regulation factor v being ubiquitously located to model excess amounts of body mass, nevertheless the advection of additional reactant v destabilises the behaviour of the growth front [70, 12]. We assume that v is advected to network nodes in amounts proportional to the conductivities D of all tubes ending at the node. Thus, we adapt equation (4.1b) to

$$\frac{\partial v}{\partial t} = (D_v \Delta v + uv^2 - \alpha_1 v) / \tau_2 + kB(w) \tilde{D}(\mathbf{x}) \quad (4.4)$$

where k is the interaction strength (for example the concentration of advected v), $\tilde{D}(\mathbf{x}_i) := \sum_j D_{ij}$ is the sum of the conductivities of the tubes ending at a node i located at \mathbf{x}_i , and $B(w)$ is the location of the growth front since we claim that the emergence of v from the tube network only occurs at the growth front:

$$B(w) = \begin{cases} 1 & w \in [w_{\text{ext}}, w_{\text{int}}] \\ 0 & \text{otherwise.} \end{cases} \quad (4.5)$$

where w_{ext} and w_{int} are constants chosen such that $w < w_{\text{ext}}$ everywhere outside the organism and $w > w_{\text{int}}$ everywhere inside the organism except at the growth front.

(2), (3) The pressure at any point in the tube network is determined by the contraction state of the actomyosin, that is, by proxy, by the local calcium concentration [89, 91]. Since this is the driver of the cytosolic flux, we include

it in equation (4.2b). In addition, the pressure change is also influenced by the stiffness of the wall which is in turn affected by the local concentration of solation factors [30, 40]. The high concentration of solation factors at the growth front and the resulting low pressure there creates a sink at the growth front. This, too, is considered in equation (4.2b) as

$$\frac{dp_j}{dt} = \sum_i \frac{1}{\tilde{C}_{ij}(D_{ij})(1 + a_v v_{ij})} q_{ij} - \kappa(c_j - \bar{c}) \quad (4.6)$$

where $v_{ij} := [v(\mathbf{x}_i) + v(\mathbf{x}_j)]/2$ is the average concentration of v in the tube between nodes i and j and a_v is a positive constant. Since the contraction in *Physarum* is small when the calcium concentration is large, we take κ to be a positive constant. $c_j := c(\mathbf{x}_j)$ is the concentration of calcium at node j and \bar{c} is the basal concentration of calcium.

(4) Finally, a rather technical point, which is a consequence of the model being set-up in two layers. Although a fine and dense grid of veins pre-exist in this implementation of the model, they are only allowed to expand their diameter to assume non-zero size when the vein is in the region occupied by the organism. Therefore, we assume that equation (4.2c) for the conductivity change depends on the organism's thickness so that tube growth can only occur inside the organism, defined by a threshold thickness:

$$\begin{aligned} \frac{dD_{ij}}{dt} &= \Gamma(w_{ij}) \frac{|q|^\mu}{1 + a_d |q|^\mu} - r D_{ij} \\ \Gamma(w) &:= \begin{cases} 1 & w > w_{th} \\ 0 & \text{otherwise} \end{cases} \end{aligned} \quad (4.7)$$

where $w_{ij} := [w(\mathbf{x}_i) + w(\mathbf{x}_j)]/2$ is the average thickness of the organism along a tube and w_{th} is the threshold thickness defining the border between 'inside' and 'outside'.

In addition to influencing each other numerically, the three model components also have to have co-ordinated time scales. The relative time scales of the contraction waves and the growth front extension, that is, the ratio between τ_1 in equations (4.3) and τ_2 in equations (4.1) was chosen such that approximately 600 contraction waves run through the body until it has extended over the whole arena, which is in concordance with experimental observations. The absolute values of τ_1 and τ_2 were chosen such that the resulting vein network visually resembles the structure in the real organism. We will revisit the latter point further down (section 4.1.4).

We used the finite element method to solve the contraction wave and the growth front dynamics, employing Neuman boundary conditions. We generated the spatial mesh (figure 4.1) by using the software FreeFEM++ [32]. The parameter values for the numerical evaluation are listed in table 4.1.

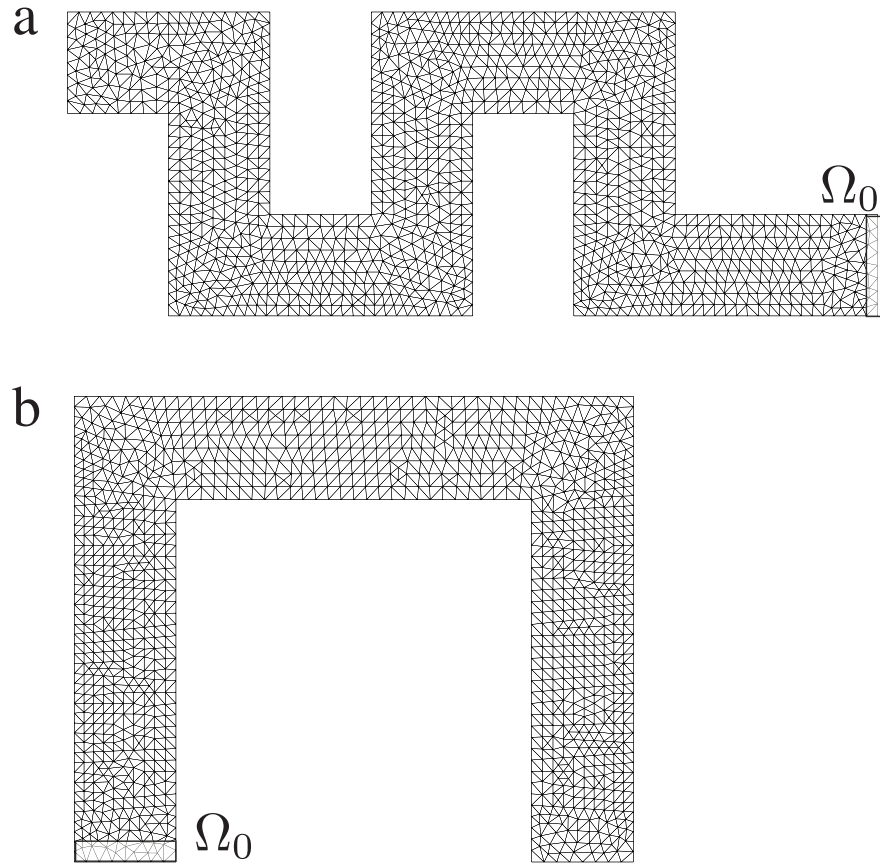


Figure 4.1: Examples for the spatial mesh generated for the evolution of the tube network. a: The snake-shaped arena. b: The U-shaped arena. Ω_0 indicates the starting position representing the location where a biological sample would be placed. Modified from [69].

The initial values for the variables are

$$\begin{aligned}
p_j(0) &= 0 \quad (j = 1, \dots, N) \\
q_{ij}(0) &= 0 \quad (i, j = 1, \dots, N) \\
D_{ij}(0) &= \begin{cases} 0.1 & \text{if } \mathbf{x}_i \in \Omega_0 \text{ or } \mathbf{x}_j \in \Omega_0 \quad (i, j = 1, \dots, N) \\ 0 & \text{otherwise} \end{cases} \\
c(\mathbf{x}, 0) &= \begin{cases} 1.0 & \mathbf{x} \in \Omega_0 \\ 0.0 & \mathbf{x} \in \Omega \setminus \Omega_0 \end{cases} \\
\varphi(\mathbf{x}, 0) &= 0 \quad \mathbf{x} \in \Omega \\
u(\mathbf{x}, 0) &= 3 \quad \mathbf{x} \in \Omega \\
v(\mathbf{x}, 0) &= \begin{cases} 1.0 & \mathbf{x} \in \Omega_0 \\ 0.0 & \mathbf{x} \in \Omega \setminus \Omega_0 \end{cases} \\
w(\mathbf{x}, 0) &= 0 \quad \mathbf{x} \in \Omega
\end{aligned}$$

where $\Omega \subset \mathbb{R}^2$ are the points within the arena and $\Omega_0 \subset \Omega$ represents the region in which the organism is initially placed (figure 4.1).

In order to generate an actomyosin contraction wave [88], we take τ_1 to be a function of space (see table 4.1). In particular, we assume that τ_1 in the starting region Ω_0 is smaller:

$$\tau_1(\mathbf{x}) = \begin{cases} \bar{\tau}_1/3, & \mathbf{x} \in \Omega_0 \\ \bar{\tau}_1, & \text{otherwise} \end{cases} \quad (4.8)$$

With this setting, a periodic contraction wave propagating from Ω_0 to the leading edge is observed. In addition, due to the interaction term $\kappa(c_j - \bar{c})$ in (4.6), a to-and-fro sol flow reminiscent of the ‘shuttle streaming’ in *Physarum* [39, 90, 73] occurs.

The components of the model are summarised visually in figure 4.2 a, and the distributions of the variables in equation (4.1) are shown in figure 4.2 b.

4.1.3 Evaluation of the model

A typical sequence of the model’s evolution is depicted in figure 4.3. It is clearly visible that the model re-creates the key features of the organism’s extension: the main veins are formed at a short distance behind the growth front; the position of the main vein, once it has emerged, remains constant over time; and the trajectory of the main vein follows a centre-in-centre pattern at each corner.

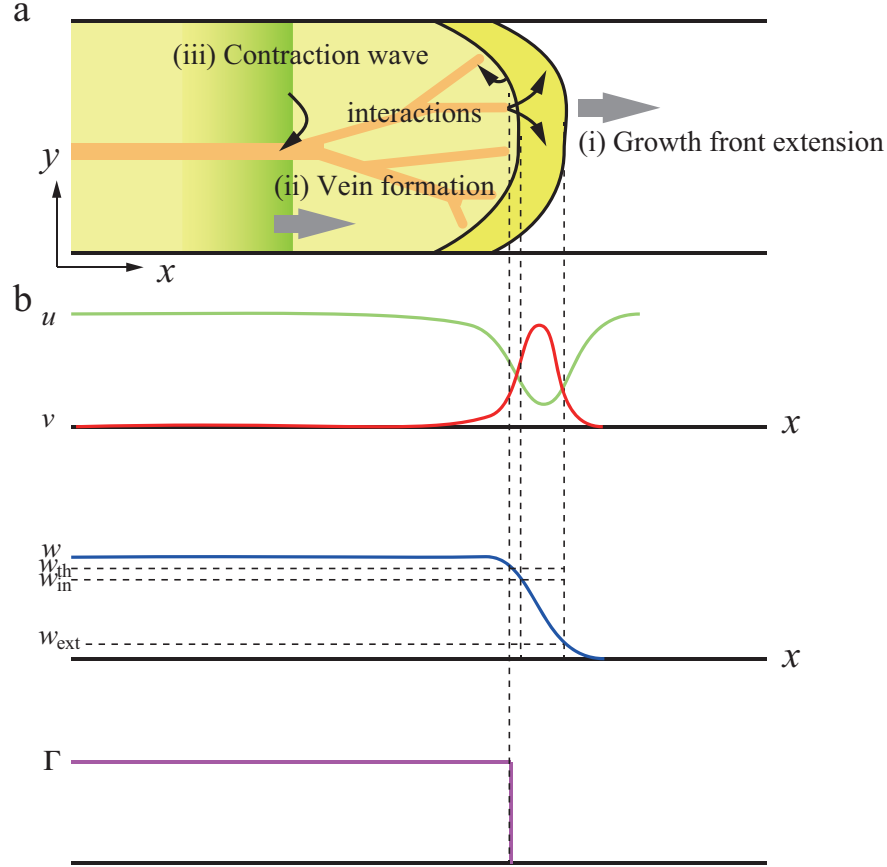


Figure 4.2: Visual summary of the numerical model. a: The main model components. b: The distributions of the solution factor v (equation (4.1b)) and the regulatory factor u (equation (4.1a)), the thickness of the organism w (equation (4.1c)), and the definition of the ‘inside’ of the organism Γ relative to the modelled processes. Modified from [69].

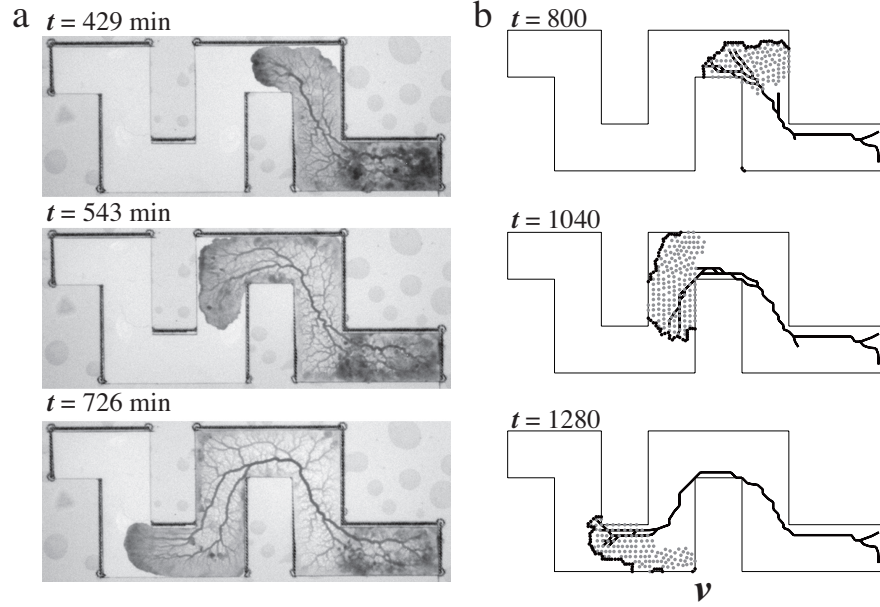


Figure 4.3: A typical sequence of the model's evolution in comparison to a time series of an experiment with the real organism. a: 3 frames from an experiment with *Physarum polycephalum* in a snake-shaped arena. Note how multiple major veins emerge after the growth front (e.g., arrow at 543min), while only those that connect to the growth front at later stages are maintained (compare to the same location at 726min). b: 3 frames from a model run. Highlighted are the growth front (thick solid line), the main vein (solid line), and the location of solation factors v (grey dots, indicating the growth zone of the organism; see text for details). Note that the model not only qualitatively recreates the trajectory, but also produces multiple veins behind the growth front, only one of which is kept later. From [69].

$a_0 =$	0.349353	$D_c =$	0.2	$w_{\text{ext}} =$	0.1
$a_1 =$	-0.0454567	$D_u =$	0.2	$w_{\text{in}} =$	0.9
$a_2 =$	1.15905	$D_v =$	0.02	$w_{\text{th}} =$	1.0
$a_3 =$	1.823858	$k =$	0.01	$\alpha_1 =$	0.01
$a_c =$	0.03	$k_E =$	0.1	$\alpha_2 =$	0.1
$a_d =$	0.01	$k_L =$	0.004	$\kappa =$	1.0
$a_i =$	5.0	$k_Q =$	1.0	$\mu =$	1.3
$\bar{a}_i =$	10.0	$k_V =$	0.12	$\bar{\tau}_1 =$	0.0072
$a_r =$	13.5	$K_* =$	1.75	$\tau_2 =$	20
$\bar{a}_c =$	0.1	$N_c =$	25.0		
$a_v =$	0.01	$r =$	0.15		
$\bar{a}_r =$	2.5	$R =$	1.0		
$\bar{c} =$	7.0				

Table 4.1: Parameter values for the numerical simulation. Values from [73, 72, 3], see also [69].

These observations are statistically stable (figure 4.4). Moreover, a comparison between the experimental data and the model data (figure 4.4) shows that the two coincide at almost all places, save for a single location where the model exhibits exceptionally low variability. However, even this deviation, while quantitatively significant, is qualitatively irrelevant, since both data show the typical centre-in-centre trajectory.

It is interesting to compare the time scales of the components of the model. The time scale of the tube development is difficult to calculate and may, in fact, have multiple time scales, depending on the geometric situation. The effective time scale of the vein formation process in the experiment can, however, be determined by fitting an exponential function through data indicative of the process. For example, the absorbance of a given piece of plasmodium decreases as that piece goes through various stages in the vein formation process concurrently with the growth front moving away. Then, the denominator of the exponent is the time scale. Thus, we could determine the effective time scale of the vein formation process to be 195 seconds (see figure 4.5). In other words, the tube network formation is not on the same time scale as the (faster) growth front extension, but the difference (a factor of roughly 10) is not so large as to call the two processes uncoupled (as is, for example, the case between the actomyosin contractions and the other two processes). In the next section, we will investigate the relevance of this ratio of the two processes' time scales.

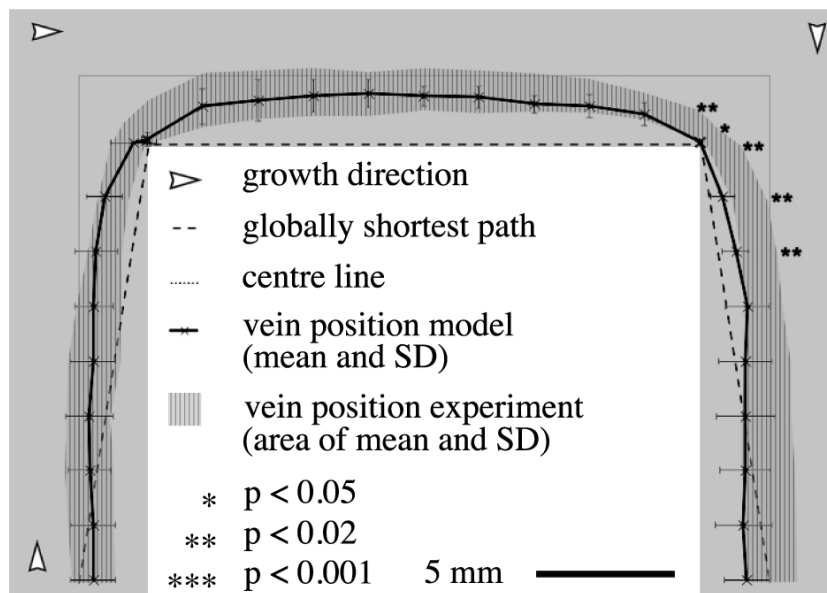


Figure 4.4: Quantitative analysis of the vein trajectory of the model. The model's main vein's position was measured at intervals equivalent to the experiment with the real organism. The average vein (solid black line with standard deviations at the measurement points) is in most parts statistically indistinguishable from the position of the real organism's vein (grey area indicating the area spanned by the standard deviation around the average position) at almost all positions. Only at the second corner there is significant difference due to the very low variation in the model's results. We also show the geometrically shortest path (broken line) and the arena's centre line (dotted line). The model exhibits the same centre-in-centre trajectory at each corner seen in the experiments with *Physarum* and is clearly different from the globally shortest path. Modified from [69].

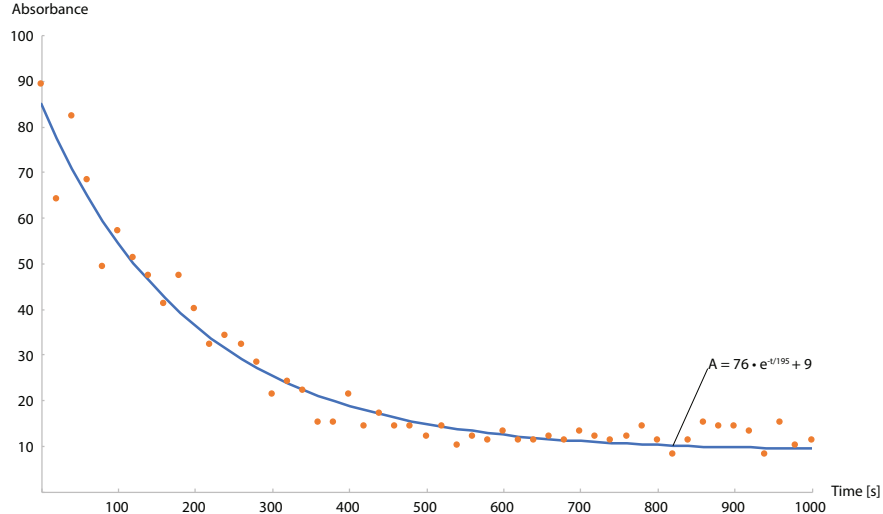


Figure 4.5: The absorbance of a given location in the plasmodium decays exponentially. This is indicative of the recruitment of body mass into the vein network as the growth front moves away. The fitting curve follows the equation $A = 76e^{-\frac{t}{195}} + 9$. Thus, the time scale of the process is 195 seconds.

4.1.4 Variation of model parameters

Now that we have established that the model is able to reproduce the natural behaviour well, it is instructive to examine its performance under different numerical conditions. We do this to investigate the importance of individual elements to the model's over-all performance and the interrelation of model components with each other. In particular, we are interested in the relevance of the interaction between growth front and vein network dynamics for the emergence of the typical centre-in-centre vein trajectory.

First, we examine the disappearance of the explicit interaction term between the vein network and the growth front. By setting k in equation (4.4) to zero, we eliminate the destabilisation of the self-propagating wave front by the advection of the solation factors through the tube network. In other words, the shape of the growth front does not any longer depend on the state of the tube network.

The result of this (figure 4.6) is that the model constructs the main vein much more closely to the globally shortest path and diverges from the experimental results more strongly and in more places. However, a centre-in-centre trajectory is still visible. This may be attributed to the fact that vein network formation still occurs in close temporal and spatial connection to the growth front extension.

Therefore, the position of the emergence of the main vein is still mainly guided by local information. But we learn that the shape of the network sensitively depends on the specific shape of the growth front.

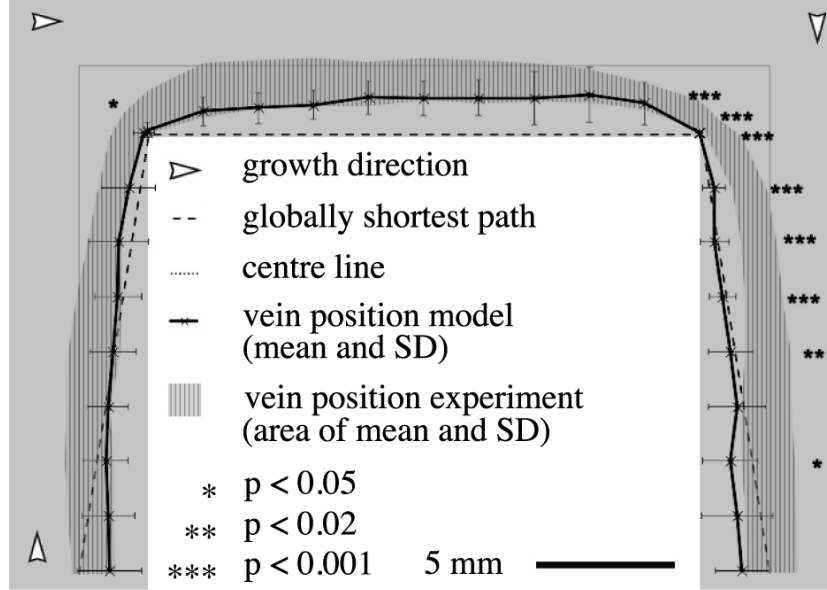


Figure 4.6: Quantitative analysis of the vein trajectory of the model with no explicit interaction between the growth front dynamics and the vein network ($k = 0$). The average vein (solid black line with standard deviations at the measurement points) is statistically different from the position of the real organism's vein (grey area indicating the area spanned by the standard deviation around the average position) at a greater number of positions. The vein's trajectory is much closer to the geometrically shortest path (broken line), but still exhibits a centre-in-centre trajectory at each corner (especially obvious in the stretch between the two turns). Modified from [69].

Next, we investigate the importance of the relative speeds (that is, time scales) of the growth front's migration speed and the vein network formation. One of the possible parameters that can control the migration speed is τ_2 in equation (4.4), the time scale of the leading edge dynamics. By decreasing τ_2 the migration speed of the growth front increases. But since we also decrease τ_1 , thus keeping the ratio between τ_1 and τ_2 constant, the number of contraction waves until full exploration is unchanged.

The over-all effect of this is that the time scale of the tube network formation is much slower relative to the modelled organism's extension and the main veins do not any longer emerge shortly behind the growth front (figures 4.7 a and b). This change has a clear and significant impact on the tube network's lay-out (figures 4.7 c and d). The main vein does now not exhibit the centre-in-centre trajectory, but runs alongside the inner boundary between the two 90° turns.

Since in this situation the network is forming in a globalised hydrodynamic regime, that is, with most of the arena's geometry accessible to the developing network, this lends heightened credibility to our assessment (section 3.2) that the centre-in-centre geometry is a product of local optimisation in the tight interplay between growth front and tube network dynamics.

4.1.5 Interpretation

It is remarkable that a simple organism like *Physarum polycephalum*, without means to perceive its distant environment, is able to produce network solutions 'on-the-go' that are close to optimal solutions even in the absence of full spatial information. It is even more remarkable that this phenomenon could only be modelled by the 'complex reduction' of available information. This is to say, the model we propose above is highly complex (even though very incomplete) in that it employs very disparate sub-models; however, the resulting whole does not integrate a greater deal of information than each of the sub-units, but rather, each sub-unit determines and, therefore, restricts the way others can unfold. For example, instead of allowing the tube network to develop over the whole space at once, the growth front grants access to the network only gradually; or, vice versa, instead of letting the growth front propagate freely, its speed was limited to the developmental time scale of the tube network.

In the real organism, *Physarum polycephalum*, these limitations are not, of course, arbitrary but a result of its physiology. In other words, the complicated model was necessary to understand the specific limitations the organism is facing and how it is overcoming them to arrive at such efficient network solutions. The answer to this seems to be that the organism couples the development of its vein network to the extension of the growth front such that current-reinforcement-based optimisation can work locally, while still allowing for the rapid construction of a tube network. This combination guarantees efficient body mass supply from and (chemical or hydrodynamic) communication with the rear of the organism.

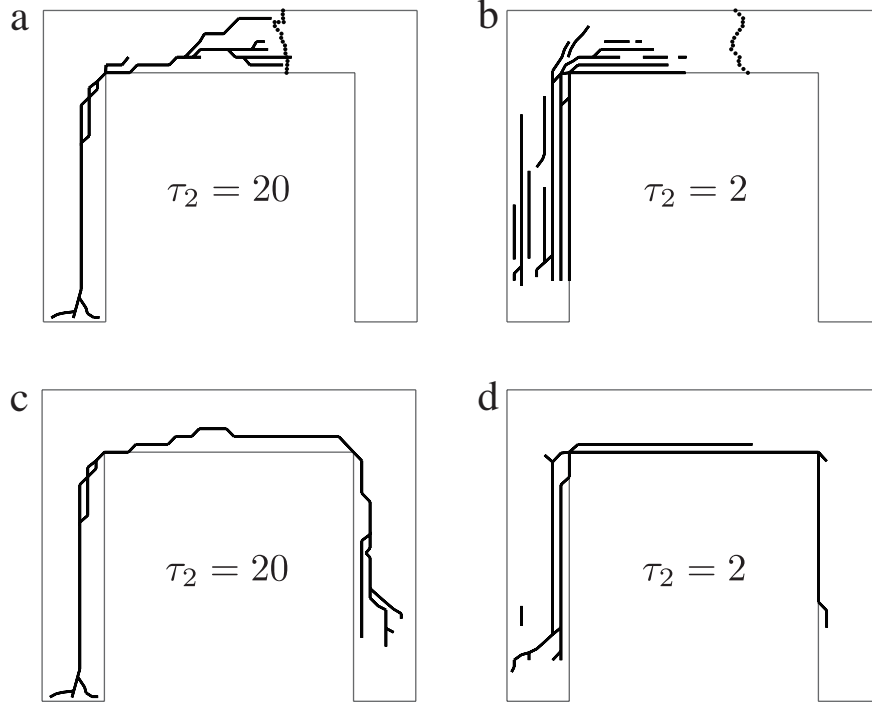


Figure 4.7: Effects of dissociating the time scale of the growth front extension from the network development. τ_2 controls the time scale of the growth front propagation relative to the vein network development. Smaller values result in a faster growth front. a: Development of the vein network under standard model conditions. Multiple veins form directly after the growth front, reducing to a single main vein at a short distance further back. b: Development of the vein network with the growth front developing on a much faster time scale than the vein network. Veins emerge only at a distance behind the growth front and, until this point in the simulation, have not yet converged to single main vein. c: Final vein lay-out under standard conditions. Note that the vein detaches from the inner boundary between the two turns. d: Final vein lay-out under dissociated conditions. The vein trajectory approaches the global optimum. Modified from [69].

4.2 Derivation of a simple algorithm to predict the vein network's lay-out

The take-away message of the above model is that the vein development is closely controlled by the growth front extension. Not only is the network's emergence spatially linked to the extension zone, it also depends sensitively on the shape of the growth front. A corollary of this finding is that growth front extension history alone should be sufficient to make a prediction on the main vein trajectory. This prediction can be made using only the quintessence of the above model: the local optimisation of vein trajectories [69].

4.2.1 Algorithm principle

If it is true that the shape of the growth front is the major determinant of the lay-out of the organism's internal tube network under extension, a series of growth front positions as it sweeps through the arena should be enough to predict, or rather, reconstruct the trajectory of the main vein. The input of the algorithm is, therefore, simply the sequence of extension front shapes (figure 4.8).

Two consecutive growth front positions are then connected tentatively by straight lines such that for each point in the later (newer) position, the closest point in the earlier (older) position is sought (figure 4.9, but see next paragraph). This follows the rationale that, during extension, a large number of proto-channels are formed in more or less straight lines outward from [29]. This process is simply repeated for all consecutive pairs of growth front positions. In the end, however, only those tentative connecting lines are kept for the final result that link up to a continuous connection from the very last (newest) growth front position to the very first (oldest) position. The idea behind this is that all channels that end blind will not continue to carry flow, and thus they will be depreciated, whereas those that continue to experience flow because they connect the organism end-to-end will not only remain, but also grow in diameter. This method will usually lead to only one remaining vein which is the prediction for the trajectory of the real organism's main vein.

In order to simplify the calculation, we run the vein prediction algorithm on an inverted time sequence of growth fronts (figure 4.9). Thus, we first calculate the shortest linear connections of all points in the last (newest) growth front to points in the growth front just before. For the next step and all steps after that, we only consider the points in the earlier (older) growth front that the algorithm has arrived at from the later (newer) growth front in the previous step. The

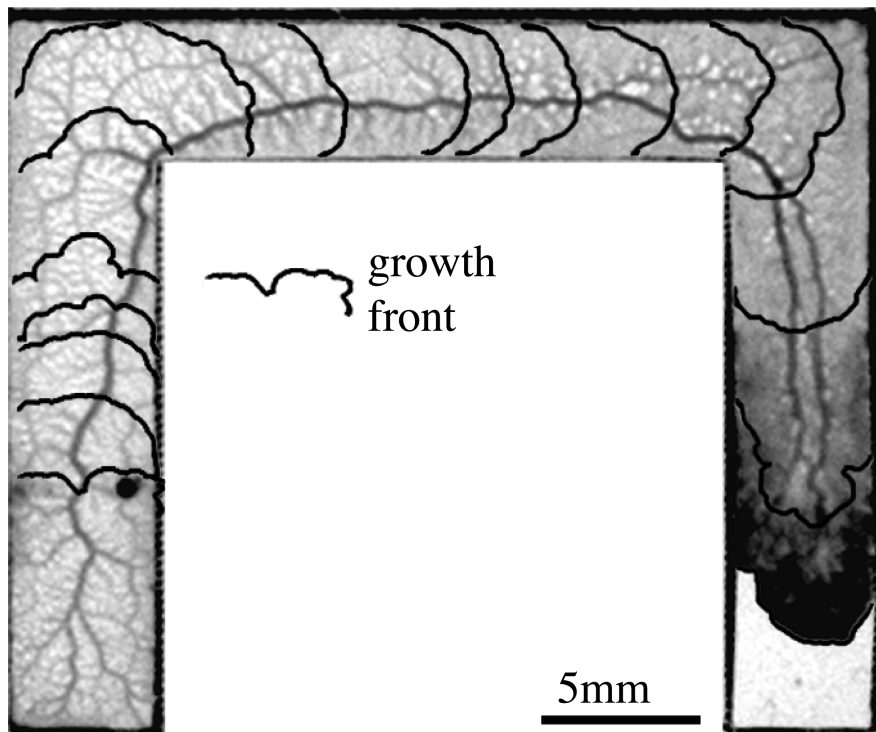


Figure 4.8: A representation of the growth front history of *Physarum polycephalum* extending through a U-shaped arena. Growth front positions are shown at 60-minute intervals. Note that the main vein seems to connect its intersection point with the later (younger) to the closest point in the earlier (older) of two consecutive growth fronts. The data used for the algorithm is are the positions of the growth fronts only. From [69].

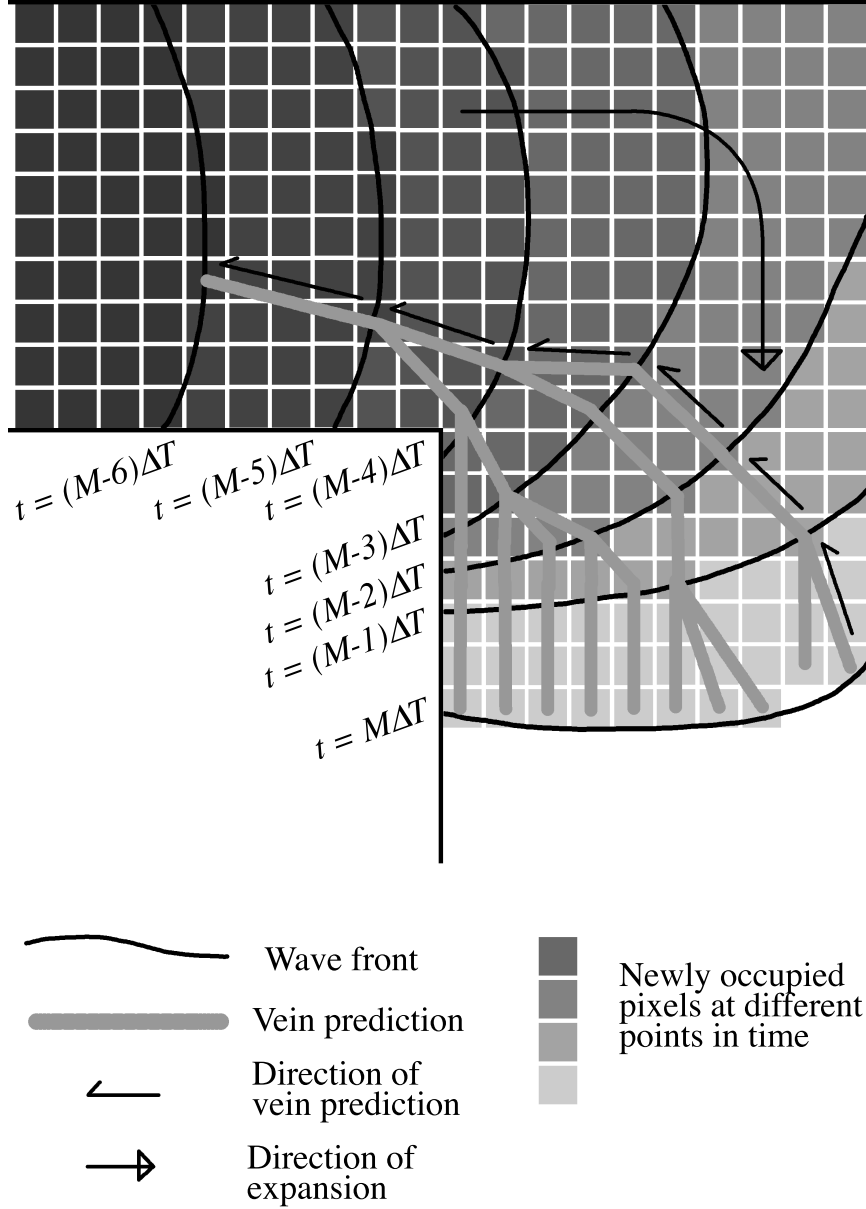


Figure 4.9: Illustration of the procedure used to obtain a prediction of the position of the main vein from the history of the expansion of the organism's growth front. The organism extends from the (top) left to the (bottom) right. The wave front is defined as the largest set of newly occupied pixels in each frame. To predict the position of the vein at $(m-1)\Delta T$, the minimal distance connection of the vein position at $m\Delta T$ to the growth front at $(m-1)\Delta T$ was determined. This was done for every frame from the last ($M\Delta T$) to the first. From [69].

rationale is that all other points in the considered growth front will not connect to the growth front after it and any connection to these points from the growth front before it will, therefore, disappear. The result is necessarily the same as in the natural time sequence. However, not all shortest connections from all points in all consecutive growth fronts have to be calculated but only those that will link up to the final growth front.

4.2.2 Evaluating the algorithm's performance

The algorithm is able to predict experimental results with remarkable accuracy (figure 4.10). Here, we used the algorithm to predict the trajectory of the main vein of a sample of *Physarum* extending through a more complicated, snake-shaped arena.

The good performance can be expressed quantitatively by the very low average distance (figure 4.11 a) of the predicted vein from the actual major vein (figure 4.11 b). By comparison, the average distance between the real vein and the shortest possible path (figure 4.11 c) is more than twice as large. This also means that the hypothesis that the organism tries to minimise its global path length is less predictive than the hypothesis that the organism's behaviour is driven by local optimisation.

In addition, the prediction algorithm also manages to accurately capture the branching pattern of the vein network directly behind the growth front, with many parallel veins coalescing into a few major veins, which finally merge into a single vein.

The data presented above are based on time differences between growth front positions of 9 minutes. However, since we took pictures of the growth front at a smaller time interval, i.e., every 3 minutes, we made the predictions using only every third picture of the full data series. Therefore, three possible predictions are possible, which we superimposed. All three predictions yielded almost identical results in all samples ($n = 8$) but one.

Figure 4.12 shows an example of a partially failed prediction. In this superimposition of three parallel predictions, based on the three different subsets that can be chosen for a time interval of 9 minutes, two of these predictions trace the actual major vein of the organism, but one prediction deviates between the third and the fourth 90° bend. Interestingly, though, this deviation traces a secondary vein that the organism did in fact construct, but dismantled shortly thereafter.

Generally, a multiplicity of veins is encountered either immediately behind the growth front or where the growth front has expanded to a wide arch, e.g. at

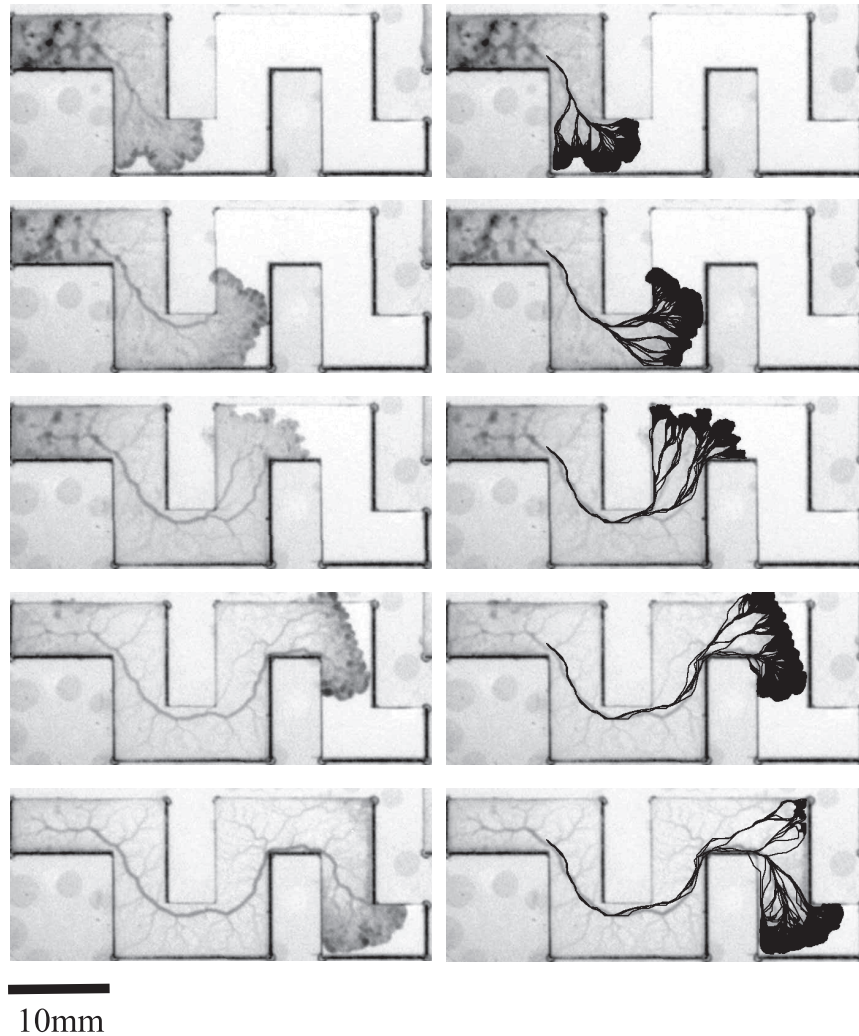


Figure 4.10: The vein prediction algorithm (right: black lines superimposed over pictures of the experimental data) predicts the position of the organism's main vein (left: experimental data) with remarkable accuracy. From [69].

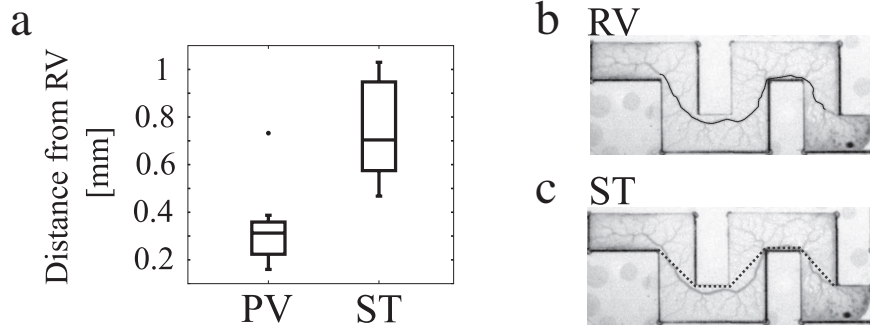


Figure 4.11: Quantitative evaluation of the performance of the vein prediction algorithm. a: Comparison between the average normal distance of each point of the predicted vein (PV) to the real vein (RV), compared to the average distance of each point of the globally shortest trajectory (ST) to the real vein. The average distance of the algorithm is less than half that of the globally shortest path, demonstrating that local optimisation yields a better prediction of the real vein's position than global optimisation. b: Highlight of the real vein's position (black line). c: Globally shortest possible path through the arena (dotted line). From [69].

a corner where a new direction for expansion opens up [29, 76]. In both cases this is due to the geometric fact that if the angle of aspect of the growth front is large from a given distance from it, local path length minimisation will require more than one end point. But both in the organism as well as in the algorithm, as the growth front moves away and refocuses, the number of paths is reduced, as many of the now disappearing veins do not connect to the growth front in an efficient way anymore. However, sometimes (usually: two) parallel veins survive, at least for an extended time [43]. This is true for the organism in a literal sense, but even in the algorithm this can occur when looking at the composite image of numerous parallel predictions based on different subsets of the same image series (as described above and shown in figure 4.12).

We interpret this occurrence as examples for situations in which, in the real organism, two veins are virtually equally efficient for supplying body mass to the growth front at one point in time, so that current reinforcement (or, in the algorithm, local path minimisation) cannot decide on one particular path. In these cases, the organism keeps both veins functional, a trait that might pay off at a later point in time, when the geometry of the environment is explored to a higher degree. Then, one of the multiple veins might be in a preferable

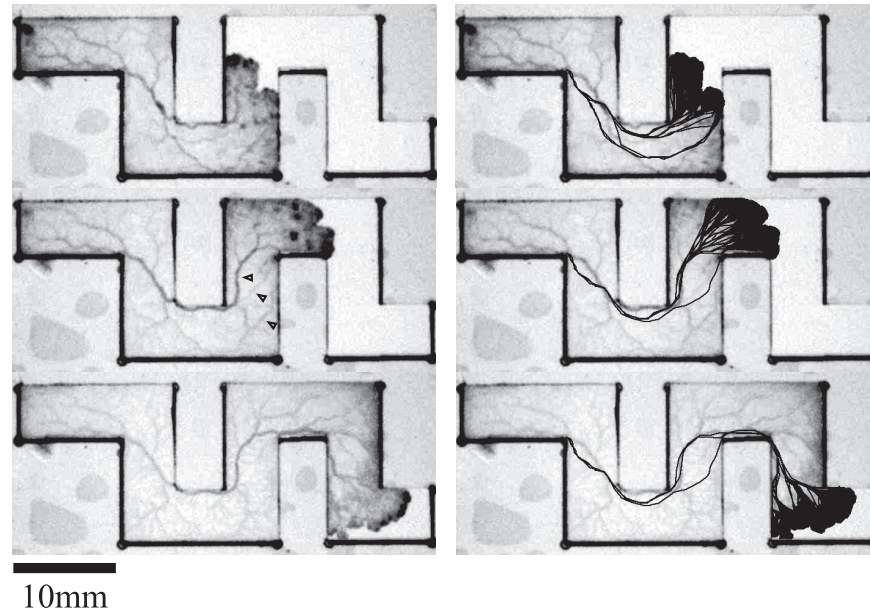


Figure 4.12: Partially failed main vein predictions. Left side: Experimental data. Right side: Algorithm results (lack lines) over-laid over experimental data. Multiple lines result from the over-laying of multiple predictions based on different sub-sets of the full growth front history. Note that the failed prediction (black arrow in the middle panel of the right column) seems to trace one of the secondary veins of the organism (small arrows in the middle panel of the left column). From [69].

position and will be used to a greater extent than the other, which will disappear as a consequence. Therefore, the appearance of a multiplicity of veins can be interpreted as an adaption to a fundamental problem of *Physarum*, that is, the lack of remote sensory abilities, and the need to entertain multiple behavioural options to be able to react to ‘unforeseen’ environmental conditions.

We also varied the time interval between growth front positions used for making the predictions. Using time intervals that are too small often fails to correctly identify the main vein. In these cases the algorithm returned predictions that retrieved the position of some secondary vein or a temporary main vein (see figure 4.12 for an example). On the other hand, if the time interval for the vein prediction is too large the accuracy of the prediction decreases (figure 4.13). This is due to the fact that the growth reacts to environmental conditions (e.g. corners or obstacles) and in turn influences the position of the vein, and this information is ignored for the frames skipped when working with large time intervals. In practice, time intervals around 15 min yielded the smallest median distance of the predicted vein from the actual major vein. However, owing to the large variation among the samples, the differences between the time intervals in figure 4.13 were not statistically significant, and we could not establish a single time interval ΔT (≤ 30 min) yielding the best result for all studied samples. We interpret this as hinting at a variability in the duration of the determination process in the organism itself, possibly depending on expansion speed and environmental conditions.

4.2.3 Conclusion

The algorithm is based on the observation that the tube network development in *Physarum* is coupled to the growth front extension and is using current reinforcement dynamics to choose between available locally optimal solution.

The good performance of the algorithm suggests that it captures a central element of the real organism’s behaviour. This is supported by the fact that its core mechanism is derived from a model incorporating physiological characteristics of *Physarum*.

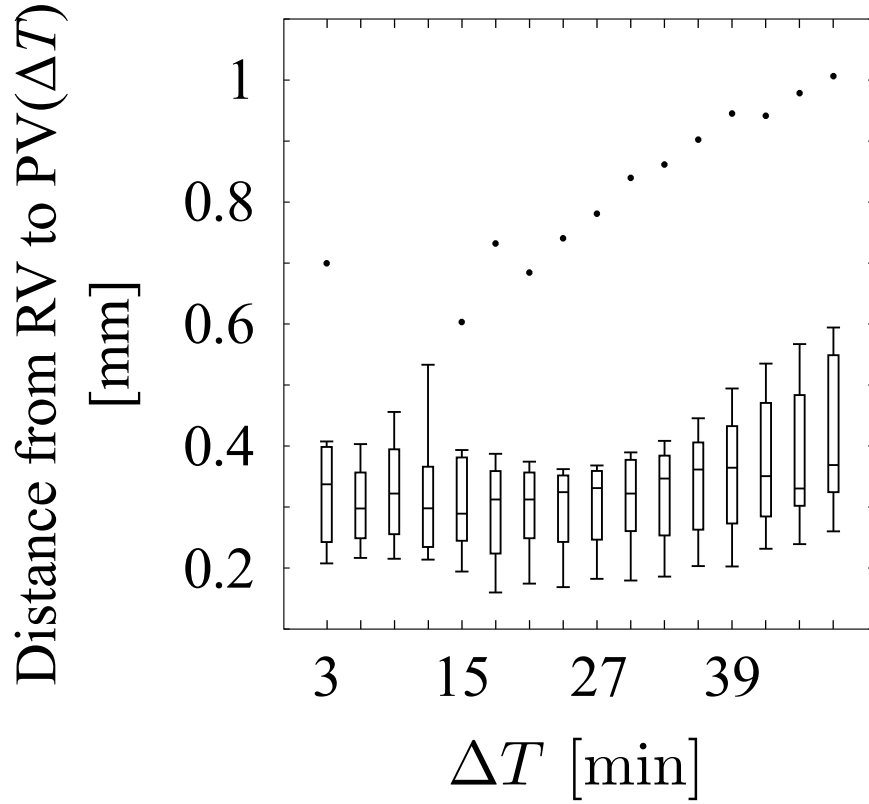


Figure 4.13: The distance of the vein prediction (PV) from the real vein (RV) , averaged over all samples, depends on the chosen frame interval. The lowest average distance is at $\Delta T = 15min$, but the large variation makes the choice of a single best time interval for all samples impossible. However, at intervals larger than 30 minutes the distance becomes larger, too. From [69].

Chapter 5

Outlook

In the preceding chapters we described how the uni-cellular slime mould *Physarum polycephalum* constructs its vein network during exploratory migration. We characterised the network in experimental studies and introduced a numerical model that integrates three physiological features that are necessary for migration and tube formation. Based on the model's success we introduced a simplified, phenomenological algorithm that draws on the model's main assumptions.

In the following, we will discuss the natural setting of this description of *Physarum* tube network development, regarding the biological reality of the organism and, briefly, the applicability of the description to other networks. We will then review which other questions are connected with the present issue.

5.1 The biological setting of the current reinforcement dynamics

The migration behaviour of *Physarum* consists of three processes: uni-directional growth front expansion [12, 29, 65], cytoplasmic streaming generated by actomyosin contraction [39, 52, 5, 80], and plasmodial vein network formation occurring in the inner part of the body [76, 12, 22]. Each of these phenomena have been described separately by mathematical models that allowed their prediction in computer simulations [75, 73, 69]. However, in nature, *Physarum* employs all three mechanisms simultaneously while foraging. As a consequence, the vein network formation depends on both the contraction waves and the growth front expansion, while the latter requires advection of protoplasm which also destabilises the wave propagation [70, 12]. Describing these three processes in concert

provides, therefore, natural boundary conditions such as coordinated temporal and spatial scales for each of the components, as well as sheds light on their interplay.

In particular, the importance of the growth front expansion for the vein network development had been neglected so far, even though it dynamically determines the area within which the vein network is to be formed. This is relevant since the static situation [81, 84, 92] yields results very different from the dynamic one (section 3.2) and is therefore an incomplete and inaccurate description of the biological situation. In addition, the global consequences of a local process such as employed by the current reinforcement model in a dynamic setting are interesting in themselves.

Under the assumptions of the static model, the food sources act as attractors for the body mass of *Physarum* and generate a directional body mass flow necessary for the current reinforcement mechanism to work, thus creating a highly efficient network connecting the food sources [82, 83]. But being spread out over a large area and then be presented with food sources placed at different positions in the area occupied is not a natural situation for the slime mould. In nature, the organism extends over surfaces and in soil in the search for food sources and amicable environmental conditions. In this process it has an incentive to transport body mass efficiently to the growth front, that is, to expend as little energy (lost due to viscous drag) as possible and to maximise extension speed [50, 77]. Here it is the expansion of the growth front, in particular the sol-gel transformation, that acts as the body mass sink causing a directional flow. Therefore, we claim that the advantage the current reinforcement mechanism confers to *Physarum* mainly lies in it affording the organism very efficient spatial exploration.

5.2 Generality of the algorithm

There are many models inspired by slime mould behaviour (for example [85, 40, 81, 37, 73, 61, 27, 57], also see [24] for a review), however, many are quite phenomenological. The benefit of the numerical model presented in this work is that it contains many parameters that physically relatable to physiological processes in *Physarum*. This allows us to study the biological meaning of and connections between the processes in the slime mould. On the other hand, because of this, the numerical model does not enjoy wide applicability.

In contrast, the derived phenomenological algorithm is based on very general principles: the local minimisation of connections and the pruning of globally disadvantageous connections due to their carrying less flow. Due to this generality,

it would be interesting to see whether the algorithmic formulation can also capture the development of other systems in which the expansion of the system's boundaries are in step with the construction of its internal network.

Can, for example, the lay-out of overland road networks be understood in terms of its contribution to the expansion of civilisation, or the growth of roots or mycelia by the flow of nutrients necessary for their construction? There are, of course, differences, as civilisations have 'remote-sensing capabilities', and roots and mycelia have no body other than the transport network (they are the transport network). Nevertheless, in all these cases the network depends on the boundaries and will develop according to flow requirements through the body, and in all these cases some form of local optimisation may yield an advantage to the efficiency of the over-all system. Therefore, it might not be unreasonable to think that the phenomenology and the mechanism discussed above are shared among a wide and significant group of natural networks, namely flow-responsive networks that form within an expanding domain.

Acknowledgements

I want to express my deep gratitude for the insightful and patient supervision by Toshiyuki Nakagaki, Kei-Ichi Ueda, Shigeru Kuroda and Katsuhiko Sato, as well as for the many inspiring discussions with other lab members and peers. Needless to say, without their guidance this work would not be. However, they also unremittingly spurred me to become a better scientist. In this vein I also want to mention the fruitful environment that was provided to me by the group of Andreas Richter and Wolfgang Wanek in Vienna, which lay the foundations of how I have been approaching science ever since.

Science is not only a tool, it is also a life style and an attitude. For allowing, supporting and actively encouraging me to live a life that enables devotion to science I am deeply indebted to my wife Ikumi and my mother Christina. I am also much obliged to the Japanese Ministry of Education, Culture, Sports, Science and Technology who have supported my life in Sapporo generously.

We stand on the shoulders of giants [59]. This is true not only for our scientific work, but also for our personal lives. We owe those giants everything.

Bibliography

- [1] Andrew Adamatzky and Jeff Jones. “Road planning with slime mould: if *Physarum* built motorways it would route M6/M74 through Newcastle”. In: *International Journal of Bifurcation and Chaos* 20.10 (2010), pp. 3065–3084.
- [2] Dai Akita et al. “Current reinforcement model reproduces center-in-center vein trajectory of *Physarum polycephalum*”. In: *Development, Growth & Differentiation* 44 (July 2017), pp. 126–6.
- [3] Dai Akita et al. “Experimental models for Murray’s law”. In: *Journal of Physics D Applied Physics* 50.2 (2017), pp. 024001–12.
- [4] Henry C Aldrich and John W Daniel. *Cell Biology of Physarum and Didymium*. Ed. by D E Buetow et al. Volume I – Organisms, Nucleus, and Cell Cycle. Academic Press, Jan. 1982.
- [5] Karen Alim. “Fluid flows shaping organism morphology”. In: *Philosophical Transactions of the Royal Society B: Biological Sciences* 373.1747 (2018).
- [6] Karen Alim et al. “Mechanism of signal propagation in *Physarum polycephalum*”. In: *Proceedings of the National Academy of Sciences* 114.20 (May 2017), pp. 5136–5141.
- [7] Karen Alim et al. “Random network peristalsis in *Physarum polycephalum* organizes fluid flows across an individual ”. In: *Proceedings of the National Academy of Sciences* 110.33 (Aug. 2013), pp. 13306–13311.
- [8] D Ambrosi, F Bussolino, and L Preziosi. “A Review of Vasculogenesis Models”. In: *Journal of Theoretical Medicine* 6.1 (2005), pp. 1–19.
- [9] M Aynsley, A C Ward, and A R Wright. “A Mathematical-Model for the Growth of Mycelial Fungi in Submerged Culture”. In: *Biotechnology and Bioengineering* 35.8 (1990), pp. 820–830.

- [10] Sandra L Baldauf et al. “A Kingdom-Level Phylogeny of Eukaryotes Based on Combined Protein Data”. In: *Science* 290.5493 (Nov. 2000), pp. 972–977.
- [11] Israel Barrantes, Jeremy Leipzig, and Wolfgang Marwan. “A Next-Generation Sequencing Approach to Study the Transcriptomic Changes During the Differentiation of *Physarum* at the Single-Cell Level”. In: *Gene Regulation and Systems Biology* 2012.6 (Oct. 2012), pp. 127–11.
- [12] Werner Baumgarten and Marcus J B Hauser. “Dynamics of frontal extension of an amoeboid cell”. In: *Epl* 108.5 (Dec. 2014).
- [13] E Bernitt, Christina Oettmeier, and Hans-Günther Döbereiner. “Microplasmidium dynamics of *Physarum polycephalum*”. In: *WCB 2010 (August 1-6)*. Berlin, Heidelberg: Springer Berlin Heidelberg, 2010, pp. 1133–1136.
- [14] S Boccaletti et al. “Complex networks: Structure and dynamics”. In: *Physics Reports-Review Section of Physics Letters* 424.4-5 (Feb. 2006), pp. 175–308.
- [15] Vincenzo Bonifaci, Kurt Mehlhorn, and Girish Varma. “*Physarum* Can Compute Shortest Paths”. In: *Journal of theoretical biology* 309 (Sept. 2012), pp. 121–133.
- [16] Graeme P Boswell et al. “The Development of Fungal Networks in Complex Environments”. In: *Bulletin of Mathematical Biology* 69.2 (July 2006), pp. 605–634.
- [17] Fabien Burki, Kamran Shalchian-Tabrizi, and Jan Pawlowski. “Phylogenomics reveals a new ‘megagroup’ including most photosynthetic eukaryotes.” In: *Biology Letters* 4.4 (Aug. 2008), pp. 366–369.
- [18] J W G Cairney. “Translocation of solutes in ectomycorrhizal and saprotrophic rhizomorphs”. In: *Mycological Research* 96.2 (Feb. 1992), pp. 135–141.
- [19] Peter Carmeliet. “Blood vessels and nerves: common signals, pathways and diseases”. In: *Nature reviews. Genetics* 4.9 (Sept. 2003), pp. 710–720.
- [20] Thomas Cavalier-Smith, Ema E Chao, and Rhodri Lewis. “187-gene phylogeny of protozoan phylum Amoebozoa reveals a new class (Cutosea) of deep-branching, ultrastructurally unique, enveloped marine Lobosa and clarifies amoeba evolution”. In: *Molecular Phylogenetics and Evolution* 99.C (June 2016), pp. 275–296.

- [21] Edward M Conway, Desire Collen, and Peter Carmeliet. “Molecular mechanisms of blood vessel growth”. In: *Cardiovascular Research* 49.3 (2001), pp. 507–521.
- [22] M Dirnberger and K Mehlhorn. “Characterizing networks formed by *P. polycephalum*”. In: *Journal of Physics D Applied Physics* 50.22 (May 2017), pp. 224002–16.
- [23] Mark Fricker, Lynne Boddy, and D Bebbber. “Network Organisation of Mycelial Fungi”. In: *Biology of the Fungal Cell*. Ed. by Richard J Howard and Neil AR Gow. Berlin, Heidelberg: Springer, Berlin, Heidelberg, 2007, pp. 309–330.
- [24] Chao Gao et al. “Does being multi-headed make you better at solving problems? A survey of *Physarum*-based models and computations”. In: *Physics of Life Reviews* (Oct. 2018), pp. 1–26.
- [25] Michael T Gastner and M E J Newman. “Shape and efficiency in spatial distribution networks”. In: *Journal of Statistical Mechanics: Theory and Experiment* 2006.01 (Jan. 2006), P01015–P01015.
- [26] Victorine B de Graaf-Peters and Mijna Hadders-Algra. “Ontogeny of the human central nervous system: What is happening when?” In: *Early Human Development* 82.4 (Apr. 2006), pp. 257–266.
- [27] Yukio-Pegio Gunji et al. “Minimal model of a cell connecting amoebic motion and adaptive transport networks”. In: *Journal of theoretical biology* 253.4 (Aug. 2008), pp. 659–667.
- [28] J Gutiérrez, A Monzón, and J M Piñero. “Accessibility, network efficiency, and transport infrastructure planning”. In: *Environment and Planning A* 30.8 (Aug. 1998), pp. 1337–1350.
- [29] Robert D Guy, Toshiyuki Nakagaki, and Grady B Wright. “Flow-induced channel formation in the cytoplasm of motile cells”. In: *Physical Review E* 84.1 (2011), pp. 016310–1–016310–13.
- [30] Takayuki Hasegawa et al. “Fragmin: A Calcium-Ion Sensitive Regulatory Factor on the Formation of Actin Filaments”. In: *Biochemistry* 19.12 (1980), pp. 2677–2683.
- [31] Luke Heaton et al. “Analysis of fungal networks”. In: *Fungal Biology Reviews* 26.1 (Apr. 2012), pp. 12–29.
- [32] F Hecht. “New development in freefem++”. In: *Journal of Numerical Mathematics* 20.3-4 (2012), pp. 1–17.

- [33] Dan Hu and David Cai. “Adaptation and Optimization of Biological Transport Networks”. In: *Physical Review Letters* 111.13 (Sept. 2013), H1706–5.
- [34] Kentaro Ito, David Sumpter, and Toshiyuki Nakagaki. “Risk management in spatio-temporally varying field by true slime mold”. In: *Nonlinear Theory and Its Applications, IEICE* 1.1 (2010), pp. 26–36.
- [35] K Ito et al. “Convergence properties for the Physarum solver”. In: *arXiv.org* (2011). scholar: 212435156640752243related:c2JgQaa48gIJ.
- [36] He Jiang and Newman L Stephens. “Calcium and Smooth-Muscle Contraction”. In: *Molecular and Cellular Biochemistry* 135.1 (1994), pp. 1–9.
- [37] Jeff Jones. “Characteristics of Pattern Formation and Evolution in Approximations of *Physarum* Transport Networks”. In: *Artificial Life* 16.2 (Apr. 2010), pp. 127–153.
- [38] Per R Jonsson and Mona Johansson. “Swimming behaviour, patch exploitation and dispersal capacity of a marine benthic ciliate in flume flow”. In: *Journal of Experimental Marine Biology and Ecology* 215.1 (July 1997), pp. 135–153.
- [39] Dietrich Kessler. “Plasmodial Structure and Motility”. In: *Cell Biology of Physarum and Didymium*. Ed. by D E Buetow et al. Academic Press, Jan. 1982, pp. 145–208.
- [40] Ryo Kobayashi, Atsushi Tero, and Toshiyuki Nakagaki. “Mathematical Model for Rhythmic Protoplasmic Movement in the True Slime Mold”. In: *Journal of Mathematical Biology* 53.2 (June 2006), pp. 273–286.
- [41] A Krogh. “The number and distribution of capillaries in muscles with calculations of the oxygen pressure head necessary for supplying the tissue”. In: *Journal of Physiology-London* 52.6 (May 1919), pp. 409–415.
- [42] Itsuki Kunita et al. “A ciliate memorizes the geometry of a swimming arena”. In: *Journal of The Royal Society Interface* 13.118 (May 2016), pp. 20160155–7.
- [43] Itsuki Kunita et al. “Adaptive Path-Finding and Transport Network Formation by the Amoeba-Like Organism *Physarum*”. In: *Natural Computing and Beyond*. Tokyo: Springer Japan, 2013, pp. 14–29.
- [44] Itsuki Kunita et al. “Shear Banding in an F-Actin Solution”. In: *Physical Review Letters* 109.24 (Dec. 2012), pp. 4866–4.

- [45] Tanya Latty and Madeleine Beekman. “Food quality and the risk of light exposure affect patch-choice decisions in the slime mold *Physarum polycephalum*”. In: *Ecology* 91.1 (Jan. 2010), pp. 22–27.
- [46] Sophie Marbach et al. “Pruning to Increase Taylor Dispersion in *Physarum polycephalum* Networks”. In: *Physical Review Letters* 117.17 (Oct. 2016), pp. 178103–5.
- [47] Felix J Meigel and Karen Alim. “Flow rate of transport network controls uniform metabolite supply to tissue”. In: *Journal of The Royal Society Interface* 15.142 (May 2018), pp. 20180075–10.
- [48] G J Mitchison. “The polar transport of auxin and vein patterns in plants”. In: *Philosophical Transactions of the Royal Society B: Biological Sciences* 295.1078 (1981), pp. 461–&.
- [49] Joyce Mohberg. “Ploidy throughout the Life Cycle in *Physarum polycephalum*”. In: *Cell Biology of Physarum and Didymium*. Ed. by D E Buetow et al. Academic Press, Jan. 1982, pp. 253–272.
- [50] Cecil D Murray. “The physiological principle of minimum work applied to the angle of branching of arteries.” In: *Journal of General Physiology* 9.6 (July 1926), pp. 835–841.
- [51] Cecil D Murray. “The Physiological Principle of Minimum Work. I. The Vascular System and the Cost of Blood Volume”. In: *Proceedings of the National Academy of Sciences* 12.3 (Mar. 1926), pp. 207–214.
- [52] Vivianne T Nachmias. “*Physarum* Myosin Light Chain One: a Potential Regulatory Factor in Cytoplasmic Streaming”. In: *Protoplasma* 109.1-2 (1981), pp. 13–21.
- [53] Toshiyuki Nakagaki, H Yamada, and M Hara. “Smart network solutions in an amoeboid organism”. In: *Biophysical Chemistry* 107.1 (2004), pp. 1–5.
- [54] Toshiyuki Nakagaki, H Yamada, and A Tóth. “Maze-solving by an amoeboid organism.” In: *Nature* 407.6803 (Sept. 2000), pp. 470–470.
- [55] Toshiyuki Nakagaki, H Yamada, and A Tóth. “Path finding by tube morphogenesis in an amoeboid organism”. In: *Biophysical Chemistry* 92.1-2 (2001), pp. 47–52.
- [56] Toshiyuki Nakagaki, H Yamada, and Tetsuo Ueda. “Interaction between cell shape and contraction pattern in the *Physarum* plasmodium”. In: *Biophysical Chemistry* 84.3 (2000), pp. 195–204.

- [57] Toshiyuki Nakagaki, Hiroyasu Yamada, and Masami Ito. “Reaction–Diffusion–Advection Model for Pattern Formation of Rhythmic Contraction in a Giant Amoeboid Cell of the *Physarum* Plasmodium”. In: *Journal of theoretical biology* 197.4 (Apr. 1999), pp. 497–506.
- [58] Toshiyuki Nakagaki et al. “Obtaining multiple separate food sources: behavioural intelligence in the *Physarum* plasmodium.” In: *Proceedings of the Royal Society B: Biological Sciences* 271.1554 (Nov. 2004), pp. 2305–2310.
- [59] Isaac Newton and Robert Hooke. “Isaac Newton letter to Robert Hooke”. Feb. 1675.
- [60] Yukinori Nishigami et al. “Influence of cellular shape on sliding behavior of ciliates”. In: *Communicative & Integrative Biology* 11.4 (Oct. 2018), pp. 1–5.
- [61] V Ntinis et al. “Modeling *Physarum* space exploration using memristors”. In: *Journal of Physics D Applied Physics* 50.17 (Mar. 2017), pp. 174004–14.
- [62] Christina Oettmeier, Klaudia Brix, and Hans-Günther Döbereiner. “*Physarum polycephalum*—a new take on a classic model system”. In: *Journal of Physics D Applied Physics* 50.41 (Sept. 2017), pp. 413001–12.
- [63] Chris R Reid and Madeleine Beekman. “Solving the Towers of Hanoi - how an amoeboid organism efficiently constructs transport networks.” In: *The Journal of experimental biology* 216.Pt 9 (May 2013), pp. 1546–1551.
- [64] V C Rideout and D E Dick. “Difference-Differential Equations for Fluid Flow in Distensible Tubes”. In: *IEEE Transactions on Biomedical Engineering* BM14.3 (1967), pp. 171–&.
- [65] Jean-Paul Rieu et al. “Periodic traction in migrating large amoeba of *Physarum polycephalum*”. In: *Journal of The Royal Society Interface* 12.106 (May 2015), pp. 20150099–20150099.
- [66] B Rodiek and Marcus J B Hauser. “Migratory behaviour of *Physarum polycephalum* microplasmodia”. In: *The European Physical Journal Special Topics* 224.7 (July 2015), pp. 1199–1214.
- [67] Anne-Gaëlle Rolland-Lagan and Przemyslaw Prusinkiewicz. “Reviewing models of auxin canalization in the context of leaf vein pattern formation in Arabidopsis”. In: *The Plant Journal* 44.5 (Nov. 2005), pp. 854–865.
- [68] T Saigusa et al. “Amoebae anticipate periodic events”. In: *Physical Review Letters* 100.1 (2008), pp. 1–5.

- [69] Daniel Schenz et al. “A mathematical model for adaptive vein formation during exploratory migration of *Physarum polycephalum*: routing while scouting”. In: *Journal of Physics D Applied Physics* 50.43 (Sept. 2017), pp. 434001–15.
- [70] Hiromi Sesaki and Satoshi Ogihara. “Protrusion of cell surface coupled with single exocytotic events of secretion of the slime in *Physarum* plasmodia.” In: *Journal of cell science* 110 (Pt 7) (Apr. 1997), pp. 809–818.
- [71] Leslie E Sieburth. “Auxin is required for leaf vein pattern in *Arabidopsis*”. In: *Plant Physiology* 121.4 (Dec. 1999), pp. 1179–1190.
- [72] D A Smith. “A Local-Oscillator Theory of Shuttle Streaming in *Physarum polycephalum* - II. Phase-Control by Cytoplasmic Calcium”. In: *Protoplasma* 177.3-4 (1994), pp. 171–180.
- [73] D A Smith and R Saldana. “Model of the Ca^{2+} oscillator for shuttle streaming in *Physarum polycephalum*”. In: *Biophysical journal* 61.2 (Feb. 1992), pp. 368–380.
- [74] W Stockem and K Brix. “Analysis of Microfilament Organization and Contractile Activities in *Physarum*”. In: *International Review of Cytology - a Survey of Cell Biology, Vol 149* 149 (1994), pp. 145–215.
- [75] Seiji Takagi et al. “Indecisive behavior of amoeba crossing an environmental barrier”. In: *Proceedings of Int ...* 2007.
- [76] Atsuko Takamatsu, Eri Takaba, and Ginjiro Takizawa. “Environment-dependent morphology in plasmodium of true slime mold *Physarum polycephalum* and a network growth model”. In: *Journal of theoretical biology* 256.1 (Jan. 2009), pp. 29–44.
- [77] Atsuko Takamatsu et al. “Energy-saving with low dimensional network in *Physarum* plasmodium”. In: *Journal of Physics D Applied Physics* 50.15 (Mar. 2017), pp. 154003–12.
- [78] Elly Tanaka and James Sabry. “Making the Connection - Cytoskeletal Rearrangements during Growth Cone Guidance”. In: *Cell* 83.2 (1995), pp. 171–176.
- [79] V A Teplov, Y M Romanovsky, and O A Latushkin. “A Continuum Model of Contraction Waves and Protoplasm Streaming in Strands of *Physarum* Plasmodium”. In: *BioSystems* 24.4 (1991), pp. 269–289.

- [80] A Tero, R Kobayashi, and Toshiyuki Nakagaki. “A coupled-oscillator model with a conservation law for the rhythmic amoeboid movements of plasmodial slime molds”. In: *Physica D: Nonlinear Phenomena* 205.1-4 (June 2005), pp. 125–135.
- [81] Atsushi Tero, Ryo Kobayashi, and Toshiyuki Nakagaki. “A mathematical model for adaptive transport network in path finding by true slime mold”. In: *Journal of theoretical biology* 244.4 (Feb. 2007), pp. 553–564.
- [82] Atsushi Tero, Ryo Kobayashi, and Toshiyuki Nakagaki. “*Physarum* solver: A biologically inspired method of road-network navigation”. In: *Physica A: Statistical Mechanics and its Applications* 363.1 (Apr. 2006), pp. 115–119.
- [83] Atsushi Tero et al. “A Method Inspired by *Physarum* for Solving the Steiner Problem”. In: *International Journal of Unconventional Computing* 6.2 (2010), pp. 109–123.
- [84] Atsushi Tero et al. “Rules for biologically inspired adaptive network design.” In: *Science* 327.5964 (Jan. 2010), pp. 439–442.
- [85] Kei-Ichi Ueda et al. “Mathematical model for contemplative amoeboid locomotion”. In: *Physical Review E* 83.2 (Feb. 2011), pp. 021916–9.
- [86] Shin Watanabe et al. “Traffic optimization in railroad networks using an algorithm mimicking an amoeba-like organism, *Physarum plasmodium*”. In: *BioSystems* 105.3 (Sept. 2011), pp. 225–232.
- [87] G B West, J H Brown, and B J Enquist. “A general model for the origin of allometric scaling laws in biology.” In: *Science* 276.5309 (Apr. 1997), pp. 122–126.
- [88] H Yamada et al. “Dispersion relation in oscillatory reaction-diffusion systems with self-consistent flow in true slime mold”. In: *Journal of Mathematical Biology* 54.6 (Jan. 2007), pp. 745–760.
- [89] Yasuaki Yoshimoto and Noburo Kamiya. “Atp-Controlled and Calcium-Controlled Contraction in a Saponin Model of *Physarum polycephalum*”. In: *Cell structure and function* 9.2 (1984), pp. 135–141.
- [90] Yasuaki Yoshimoto and Noburo Kamiya. “Studies on Contraction Rhythm of Plasmodial Strand III. Role of Endoplasmic Streaming in Synchronization of Local Rhythms”. In: *Protoplasma* 95.1-2 (1978), pp. 111–121.

- [91] Yasuaki Yoshimoto, F Matsumura, and Noburo Kamiya. “Simultaneous Oscillations of Ca^{2+} Efflux and Tension Generation in the Permealized Plasmodial Strand of *Physarum*”. In: *Cell Motility* 1.4 (1981), pp. 433–443.
- [92] Mingchuan Zhang et al. “A Novel *Physarum*-Inspired Routing Protocol for Wireless Sensor Networks”. In: *International Journal of Distributed Sensor Networks* 9.6 (Jan. 2013), pp. 483581–12.